Summary Technical Report

63-1-5

On

An Investigation of the Crack-Propagation Resistance of High-Strength Alloys and Heat-Resistant Alloys

By

J. D. Morrison
P. C. Jenkins
J. R. Kattus

November 21, 1962

Prepared under Bureau of Naval Weapons
Contract NOw 61-0392-d

23 December 1960 through 23 October 1962

Summary Technical Report

On

An Investigation of the Crack-Propagation Resistance of High-Strength Alloys and Heat-Resistant Alloys

By

J. D. Morrison
P. C. Jenkins
J. R. Kattus

November 21, 1962

Prepared under Bureau of Naval Weapons
Contract NOw 61-0302-d

23 December 1960 through 23 October 1962

Southern Research Institute
Birmingham, Alabama
5603-1256-X

FOREWORD

This is the summary technical report covering the work done during the period from December 23, 1960, through October 23, 1962, on Contract NOw 61-0302-d for the Bureau of Naval Weapons. The program was monitored by Mr. G. M. Yoder, RRMA-223, Head, Steels Unit, Bureau of Naval Weapons.

The authors acknowledge the significant contributions made to the program by the following personnel at Southern Research Institute:

1. F. R. O'Brien, Assistant Director
2. O. V. Rogers, Associate Engineer
3. W. R. Salzman, Assistant Metallurgist
4. M. A. Campbell, Assistant Metallurgist

The guidance and cooperation of Mr. G. M. Yoder and Mr. Joseph Maltz, of the Bureau of Naval Weapons, are gratefully acknowledged.

ABSTRACT

The purpose of this program was to determine the crack-propagation resistance of super-alloy and refractory-metal sheet materials and to investigate certain aspects of the elevated-temperature mechanical behavior of high-strength low-alloy steels. Sheet specimens containing central transverse fatigue cracks were used in the experimental work. It was found that the fracture toughness of the nickel-base alloys—Rene' 41, Nimonic 90, Inconel-X, and Unitemp 1753—decreased slightly in the temperature range from about 1000° F to 1400° F, in which temperature range there were generally increases in ultimate tensile strength and decreases in tensile elongation. The alloys A286 (iron-base) and L605 (cobalt-base) did not show this brittleness tendency. Among the refractory metals, unalloyed molybdenum was found to have a brittle-ductile transition temperature of about 150° F; the molybdenum alloys—Mo-1/2%Ti and TZM—both had transition temperatures of about 65° F. Unalloyed tungsten sheet, containing sharp notches rather than fatigue cracks, showed an increasing tendency to brittleness below about 500° F. Two columbium-base alloys—D-14 and FS82—were ductile over the temperature range investigated—from -320° F to about 1000° F. In an investigation of apparent strain-aging effects in steels, it was found that greatly increasing the rate of loading diminished the net-fracture-stress minimum that occurs at around 300° F at slow loading rates.

The program also included an evaluation of the compliance gage, originally developed at the U.S. Naval Research Laboratory, for the determination of critical crack length. It was found that, by means of this device, critical crack length can be reproducibly measured in crack-propagation tests over a wide temperature range. Used with certain types of crack-propagation specimens, such as the shear-cracked specimen, the gage apparently gives a reliable measure of the plane-strain fracture-toughness parameters, K_{Ic} and G_{Ic}.

TABLE OF CONTENTS

Section		Page
I	INTRODUCTION	1
II	MATERIALS	2
III	SPECIMENS	2
IV	EQUIPMENT AND PROCEDURE	7
V	RESULTS AND DISCUSSION	10
	A. Super Alloys	11
	B. Refractory Metals	16
	C. Strain-Aging Effects in Steels	23
VI	COMPLIANCE-GAGE EXPERIMENTS	31
	A. 300 M	35
	B. AISI 4340	37
	C. 7075-T6, K_{Ic} Experiments	38
VII	CONCLUSIONS	41
VIII	RECOMMENDATIONS	42
	BIBLIOGRAPHY	44
	APPENDIX A	46
	APPENDIX B	92

LIST OF ILLUSTRATIONS

Figure No.		Page
1	Typical fatigue-cracked specimen for determination of crack-propagation properties	5
2	Diagram of centrally notched and fatigue-cracked sheet specimen for compliance measurements with clip-on deflection gage in place	6
3	Sheet tensile specimen	8
4	Effect of temperature on the standard tensile properties and net fracture stress of longitudinal specimens of aged Inconel-X	11
5	Effect of temperature on the standard tensile properties and net fracture stress of aged Rene' 41	12
6	Effect of temperature on the standard tensile properties and net fracture stress of Unitemp 1753	12
7	Effect of temperature on the standard tensile properties and net fracture stress of aged Nimonic 90	13
8	Effect of temperature on the tensile-strength properties and net fracture stress of Aged A 286 alloy sheet	14
9	Effect of temperature on the tensile-strength properties and net fracture stress of annealed L 605 cobalt-base alloy sheet	15
10	Ultimate strength, yield strength, net fracture stress of unalloyed annealed tungsten sheet as functions of temperature	16
11	Effect of temperature on the standard tensile properties and net fracture stress of annealed longitudinal specimens of unalloyed molybdenum sheet	17

LIST OF ILLUSTRATIONS (Continued)

Figure No.		Page
12	Effect of temperature on the standard tensile properties and net fracture stress of annealed longitudinal sheet specimens, 0.060 in. thick, of Mo 0.5%-Ti material	18
13	Effect of temperature on the standard tensile properties and net fracture stress of annealed longitudinal sheet specimens, 0.060 in. thick of TZM molybdenum alloy	19
14	Ultimate strength, yield strength, and net fracture stress of cold-rolled and stress-relieved 0.050 in. thick D-14 columbium alloy sheet as functions of temperature	20
15	Ultimate strength, yield strength, and net fracture stress of stress-reliefed FS 82 columbium alloy sheet as functions of temperature	22
16	Effect of temperature on the standard tensile strength properties and fracture strength properties of quenched and tempered AISI 4130 sheet steel at a nominal strain rate of 1×10^{-5} in. /in. /sec	26
17	Effect of temperature on the standard tensile strength properties and fracture strength properties of quenched and tempered AISI 4130 sheet steel at a nominal strain rate of 5×10^{-3} in. /in. /sec	26
18	Effect of temperature on the standard tensile strength properties and fracture strength properties of quenched and tempered AISI 4130 sheet steel at a nominal strain rate of 0.5 in. / in. /sec	26
19	Ultimate tensile strength of tempered AISI 4130 steel sheet at different temperatures and three different strain rates	27
20	Net fracture stress of tempered AISI 4130 steel sheet at different temperatures and three different loading rates	28

LIST OF ILLUSTRATIONS (Continued)

Figure No.		Page
21	Effect of temperature on the standard tensile strength properties and fracture strength properties of hot-rolled AISI 1020 steel sheet at a nominal strain rate of 0.2 in./in./sec	30
22	Effect of temperature on the standare tensile strength properties and fracture strength properties of hot-rolled AISI 1020 steel sheet at a nominal strain rate of 1×10^{-5} in./in./sec	30
23	Ultimate tensile strength of hot-rolled AISI 1020 steel sheet as a function of temperature at two different strain rates	30
24	Net fracture stress of fatigue-cracked hot-rolled AISI 1020 steel sheet as a function of temperature at two different loading rates	30
25	Compliance as a function of crack length curve derived from the Irwin-Westergaard equation. Also shown are experimental compliances measured at low stress levels	34
26	Compliance as a function of crack length calibration curve. Compliance measurements made at 70-80% of stress required to cause crack extension	34
27	Compliance as a function of crack length curve derived from the Irwin-Westergaard equation. Also shown are experimental compliances measured at low stress levels for specimens of AISI 1020 and 300 M steels	35
28	Effect of temperature on the standard tensile properties and crack-propagation properties of 300 M steel heat treated to 240 ksi nominal yield strength level	36
29	Compliance curve for shear-crack specimen of 7075-T6 aluminum sheet, showing crack pop-in displacement	40

LIST OF TABLES

Table No.		Page
1	Refractory Metals and Super Alloys Evaluated	3
2	Sources and Chemical Composition of Refractory Metals and Super Alloys	4
3	Source and Composition of AISI 4130 Steel	5
4	Tensile Properties of Aged Inconel-X Sheet at Different Temperatures and a Nominal Strain Rate of 5×10^{-3} in. /in. /min	47
5	Fracture Strength of Fatigue-Cracked, Aged Inconel-X Sheet at Different Temperatures	49
6	Tensile Properties of Aged Rene' 41 Sheet at Different Temperature and at a Nominal Strain Rage of 5×10^{-3} in. /in. /mm	50
7	Fracture Strength of Fatigue-Cracked, Aged Rene' 41 Sheet at Different Temperatures	51
8	Tensile Properties of Aged Unitemp 1753 Sheet at Different Temperatures and at a Nominal Strain Rate of 5×10^{-3} in. /in. /min	52
9	Fracture Strength of Fatigue-Cracked, Aged Unitemp 1753 Sheet at Different Temperatures	53
10	Tensile Properties of Aged Nimonic 90 Sheet at Different Temperatures and at a Nominal Strain Rate of 5×10^{-3} in. /in. /min	54
11	Fracture Strength of Fatigue-Cracked, Aged Nimonic 90 Sheet at Different Temperatures	55
12	Tensile Properties of Aged A286 Alloy Sheet at Different Temperatures and at a Nominal Strain Rate of 0.005 in. /in. /min	56
13	Fracture Strength of Fatigue-Cracked, Aged A 286 Alloy Sheet at Different Temperatures	57

LIST OF TABLES (Continued)

Table No.		Page
14	Tensile Properties of Annealed L 605 Cobalt-Base Alloy Sheet at Different Temperatures	58
15	Fracture Strength of Fatigue-Cracked Annealed L 605 Cobalt-Base Alloy Sheet at Different Temperatures	59
16	Tensile Strength Properties of Unalloyed Tungsten Sheet at Various Temperatures	60
17	Fracture Strength Properties of Sharply Notched Unalloyed Tungsten Sheet	61
18	Tensile Properties of Unalloyed Molybdenum Sheet at Different Temperatures and at a Nominal Strain Rate of 5×10^{-3} in. /in. /min	62
19	Fracture Strength Properties of Fatigue-Cracked Unalloyed Molybdenum Sheet at Different Temperatures and at a Crosshead-Travel Rate of 0.01 in. /min	63
20	Tensile Properties of Molybdenum 1/2%-Titanium Alloy Sheet at Different Temperatures and at a Nominal Strain Rate of 5×10^{-3} in. /in. /min	64
21	Fracture Strength of Fatigue-Cracked Molybdenum 0.5%-Titanium Alloy Sheet at Different Temperatures and at a Crosshead-Travel Rate of 0.01 in. /in. /min	65
22	Tensile Properties of Molybdenum 0.5%-Titanium 0.08%-Zirconium Alloy Sheet at Different Temperatures and at a Nominal Strain Rate of 5×10^{-3} in. /in. /min	66
23	Fracture Strength of Fatigue-Cracked Molybdenum 0.5%-Titanium 0.08%-Zirconium Alloy Sheet at Different Temperatures and at a Crosshead-Travel Rate of 0.01 in. /min	67

LIST OF TABLES (Continued)

Table No.		Page
24	Standard Tensile Properties of D-14 Columbium Alloy Sheet at Various Temperatures	68
25	Fracture Strength of Fatigue-Cracked D-14 Sheet at Various Temperatures	71
26	Standard Tensile Properties of FS 82 at Various Temperatures	73
27	Fracture Strength of Fatigue-Cracked FS 82 Sheet at Various Temperatures	75
28	Tensile Properties of Tempered AISI 4130 Steel at Different Temperatures and at a Strain Rate of 1×10^{-5} in. /in. /sec	76
29	Tensile Properties of Tempered AISI 4130 Steel at Different Temperatures and a Strain Rate of 5×10^{-3} in. /in. /sec	77
30	Tensile Properties of Tempered AISI 4130 Steel at Different Temperatures and at a Strain Rate of 0.5 in. /in. /sec	79
31	Fracture Strength of Fatigue-Cracked Tempered AISI 4130 Steel at Different Temperatures and a Loading Rate of 4 lbs/sec	81
32	Fracture Strength of Fatigue-Cracked Tempered AISI 4130 Steel at Different Temperatures and a Loading Rate of 2×10^{3} lb/sec	82
33	Fracture Strength of Fatigue-Cracked Tempered AISI 4130 Steel at Different Temperatures and a Loading Rate of 2×10^{5} lbs/sec	83
34	Tensile Properties of Hot-Rolled AISI 1020 Steel Sheet at Various Temperatures at a Nominal Strain Rate of 0.2 in. /in. /sec	84

LIST OF TABLES (Continued)

Table No.		Page
35	Fracture Strength of Fatigue-Cracked, Hot-Rolled AISI 1020 Steel Sheet at Different Temperatures and a Nominal Loading Rate of 2×10^{-5} lb/sec	85
36	Tensile Properties of Hot-Rolled AISI 1020 Steel Sheet at Various Temperatures at a Nominal Strain Rate of 1×10^{-5} in./in./sec	86
37	Fracture Strength of Fatigue-Cracked, Hot-Rolled AISI 1020 Steel Sheet at Different Temperatures and a Nominal Loading Rate of 4 lb/sec	87
38	Standard Tensile Properties of 300 M Low-Alloy Steel at Various Temperatures	88
39	Crack-Propagation Properties of 300 M Low-Alloy Steel at Various Temperatures	89
40	Standard Tensile Properties of AISI 4340 Steel at 350° F	90
41	Crack-Propagation Properties of AISI 4340 Steel at 350° F	91

An Investigation of the Crack-Propagation Resistance of High-Strength Alloys and Heat-Resistant Alloys

I. INTRODUCTION

The purposes of this program were as follows:

1. To investigate the crack-propagation behavior of "super-alloy" sheet materials, particularly at elevated temperatures near the usual aging range for many of these alloys. It was expected that additional precipitation occurring during stress application at elevated temperatures could be a potential source of brittleness in the super alloys.

2. To determine the effects of pre-existing cracks on the mechanical behavior of some of the commercially available refractory-metal sheet materials, in particular, to determine their brittle-ductile transition temperatures. These data would furnish a base-line for comparison with the properties of materials subsequently produced in the Refractory Metal Sheet Rolling Program.

3. To investigate further the apparent "strain-aging" effects previously found to occur in crack-propagation tests of low-alloy steels. These effects were manifested by a minimum in net fracture stress in a temperature range (about 300° F to 400° F) within which there was a maximum in ultimate tensile strength. In general, strain-aging effects are attributed to interactions that occur in bcc metals between dislocations and interstitial atoms. Therefore, it was anticipated that such effects might be evidenced in the mechanical behavior of the refractory metals studied in this program.

In the course of the program, the development was announced by the U. S. Naval Research Laboratory of a method for measuring the extent of slow crack growth in crack-propagation determinations.

The method employed a sensitive deflectometer that measured the compliance—the extension per unit load—of specimens containing cracks or notches. A modified form of this device was developed at Southern Research Institute and was used in the evaluation of the crack-propagation resistance of a number of sheet materials in the latter part of this program.

II. MATERIALS

In Table 1 is shown a list of the super-alloys and refractory metals evaluated in the program, the sheet thicknesses, and the conditions of heat-treatment in which the materials were evaluated. Table 2 shows the sources and compositions of these materials. Several steels and one aluminum alloy used in connection with special experiments, described in subsequent sections of the report, are not included in this list. Particulars on the condition of these latter materials are given in the appropriate section.

III. SPECIMENS

Figure 1 shows the crack-propagation specimen used in the evaluation of the super-alloys and most of the refractory-metal alloys. The "lugged" crack propagation specimen shown in Figure 2 is a modification of this original fatigue-cracked specimen, and was designed for use with a clip-on deflection gage. This deflection gage is shown in place on the specimen in Figure 2, and its use is described in detail in a later section of this report. The gage was not developed until the latter part of this program; consequently, its use was limited to the evaluation of only a few materials. Both types of crack-propagation specimens contain central transverse slots, made with a jeweler's saw, the slots terminating in natural cracks which are produced by cyclic axial stressing of the slotted specimens. The critical dimensions of these specimens are as recommended by the ASTM Committee on Fracture Testing of High Strength Sheet Materials (1)[1]. The basic requirements are as follows:

1. The specimen width-to-thickness ratio should be within the limits from 16-to-1 to 45-to-1.

---

[1] Numbers in parentheses refer to the bibliography.

Table 1

Refractory Metals and Super Alloys Evaluated

Material	Sheet Thickness, in.	Condition
Unalloyed Molybdenum	0.060	Hot rolled, stress relieved
Mo 0.5%-Ti	0.060	Hot rolled, stress relieved
Mo 0.5%-Ti 0.08% Zr (TZM)	0.060	Hot rolled, stress relieved
Tungsten arc-melted	0.040	Prepared by standard powder-metallurgy technique pressed, sintered, forged, and rolled, annealed 25 min at 1830° F
Columbium D-14	0.050	Cold-rolled, stress relieved
FS 82	0.040	Hot rolled; stress relieved at 1150° C for 20 min
Rene' 41	0.060	Solutioned 1950° F, 30 min, WQ, aged at 1400° F for 16 hr, AC
Nimonic 90	0.050	Solutioned (in argon) 1975° F, 8 hr, AC, aged 1300° F, 16 hr, AC
Inconel-X	0.087	Solutioned (in argon) 2150° F, 4 hr, AC, aged 1300° F, 20 hr, AC
Unitemp 1753	0.060	Solutioned (in argon) 1975° F, 4 hr, AC, aged 1400° F, 2 hr, AC
L 605	0.045	Annealed
A 286	0.040	Solutioned 1800° F, 1 hr, OQ, Aged 1325° F, 16 hr, AC

Table 2

Sources and Chemical Composition of Refractory Metals and Super Alloys

Alloy	Manufacturer	As-Received Condition	Chevron Elements								Chemical Composition Percent of Remaining Present												
			Q	W	M	C	Mn	Si	S	P	Cr	Mo	Co	Ti	Al	Fe	B	Zr	Cb	Ni	Ta	W	Other
Unalloyed Molybdenum (Heat # M 1369)	Universal Cyclops Steel Corporation	Hot rolled stress relieved, 1650° F, 1 hr	15.0	15.0	2.0	0.050						Bal											
Mo + 0.5% Ti (Heat # KDTM 9828)	Universal Cyclops Steel Corporation	Hot rolled stress relieved, 2000° F, 1 hr	15.0	15.0	1.8	0.050						Bal		0.45									
Mo + 0.5%-Ti + 0.08% Zr (Heat # KDTZM 318)	Universal Cyclops Steel Corporation	Hot rolled stress relieved, 2000° F, 1 hr	15.0	24.0	4.2	0.015						Bal		0.45				0.20					
Unalloyed Tungsten (Lot # of Tungsten Powder W-2)	Wah Chang Corporation	Pressed, sintered, forged, and rolled; annealed 25 min at 1650° F	25	25	2.0							Bal											
D-14 Columbium	Pigments Department of E. I. duPont de Nemours & Co.	Cold-rolled, stress relieved	194	22	3	0.0011													4.5		Bal		
FS-82 (Production # 27607-6) (Lot # 82A-319)	Fansteel Metallurgical Corp.	Hot rolled, stress relieved	519	69		0.004						0.005							0.20		Bal	24.20	
Rene' 41 (Heat # R-154)	General Electric Metallurgical Prod. Dept.	Solutioned 1975° F 4 hr, WQ				0.08	0.08	0.06	0.007		18.70		9.24	10.04	3.13	1.48	0.0020		3.11	Bal			
Nimonic 80 (Heat # HT-716C)	International Nickel Co., Inc.	Cold rolled and annealed[1]				0.07	0.40	0.22	0.007		20.20			17.04	2.01	1.20	0.01		4.20	2.70			
Unitemp 1753 (Heat # KH-615)	Universal Cyclops Steel Corporation	Cold rolled, annealed and pickled				0.21	0.02	0.07	0.005	0.020	14.77	6.20	1.30	7.40	2.10	1.20	0.007	0.044	6.20	Bal			
Inconel-X (Heat # HT-3488X)	International Nickel Co., Inc.	Cold rolled, and annealed				0.04	0.72	0.20			15.20				2.51	6.20		Ta+Cb 1.00	0.40	72.60			
L 605						0.09	1.20	0.40			19.90	14.20		Bal					2.75	10.20			
A 286											15.0		1.20		2.0	0.20				Bal		25.0	

[1] Annealing for Nimonic 80: 2000° F for 10 min, quench in water-aloxed.

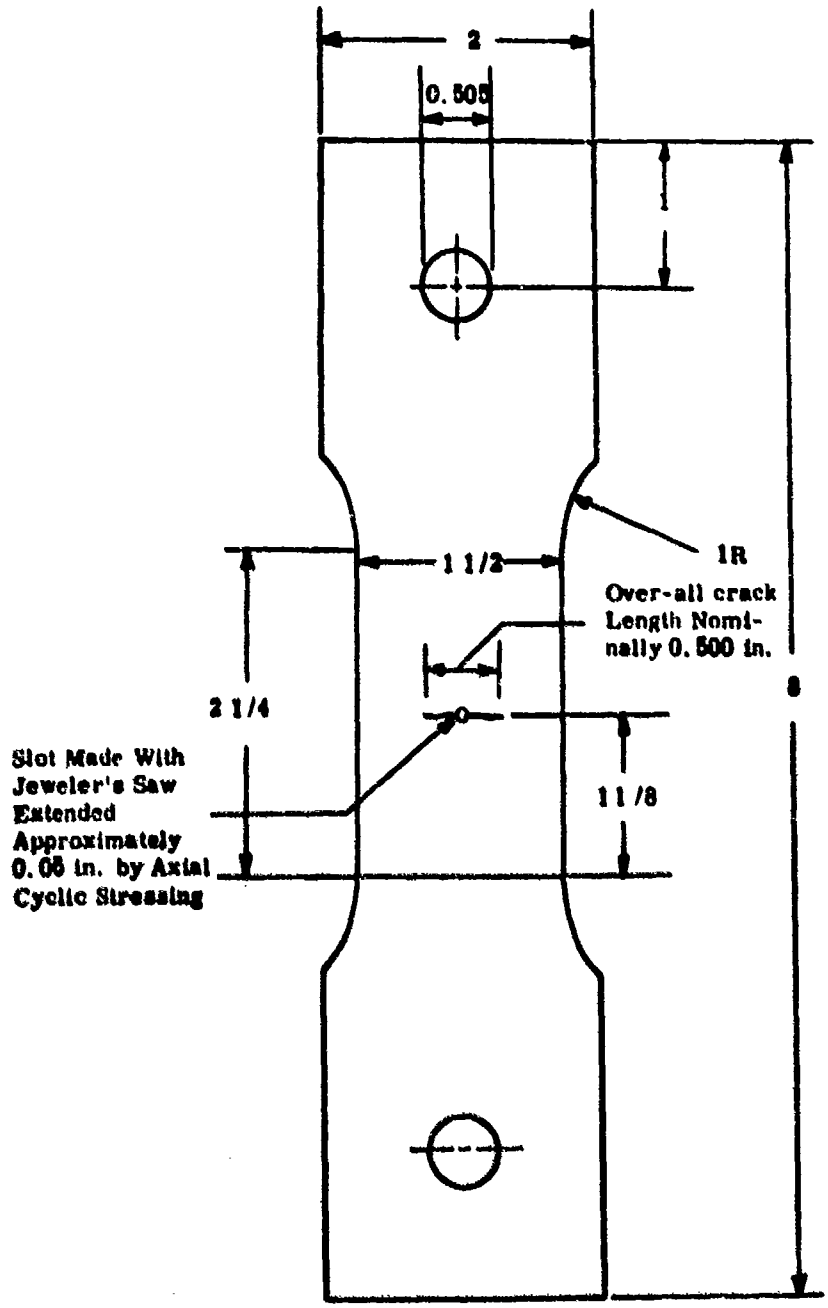

Figure 1. Typical fatigue-cracked specimen for determination of crack-propagation properties.

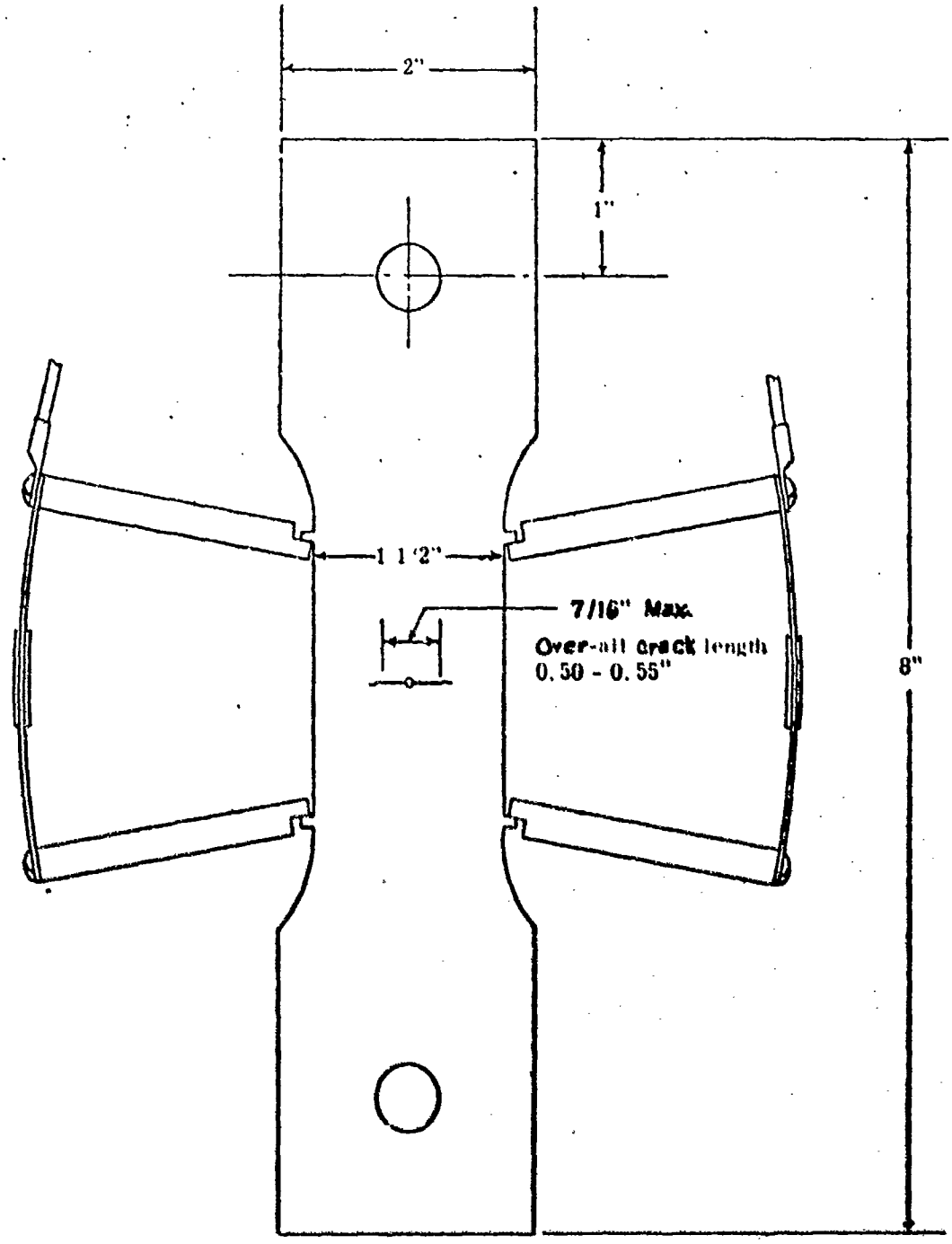

Figure 2. Diagram of centrally notched and fatigue-cracked sheet specimen for compliance measurements with clip-on deflection gage in place.

2. The distance between the centers of the loading-pin holes should be at least 2.5 times the specimen width.

3. The initial over-all crack length should be from 0.3 to 0.4 of the over-all specimen width.

Standard tensile specimens of each material were also evaluated. A typical tensile specimen is shown in Figure 3. In some instances the over-all length of these specimens was reduced to conserve the materials of limited availability, but the dimensions of the gage section remained the same for all the materials. These specimens have machined "lugs" at the 2-in gage points for actuating a special clip-on extensometer, which can be used for measuring strain over a wide range of specimen temperatures.

IV. EQUIPMENT AND PROCEDURE

A special screw-type tensile loading machine, designed and built at Southern Research Institute, was used for determining the standard tensile properties of the sheet materials and the crack-propagation properties when rapid loading rates were required. With this machine, a range of strain rates from 0.00005 in./in./sec to 1.0 in./in./sec can be obtained for standard tensile specimens of 2-in. gage length. Strain gages are used as the transducers on both the load cell and extensometer, which produce electrical signals proportional to the load and to the strain within the 2-in. gage section of the specimen. The stress-strain curves are photographed by a Polaroid-Land camera from a cathode-ray oscilloscope. A detailed description of this equipment is contained in WADC TR 57-649. When rapid loading rates were not required, the crack-propagation specimens were loaded to failure in a Tinius Olsen testing machine of 120,000 lbs capacity at a free crosshead-travel rate of about 0.01 in./min.

Specimen temperature for both the fatigue-cracked specimens and standard tensile specimens was obtained in the following ways. For the low-temperature work, the central 3-in. section of the specimen was enclosed in an insulated cold-box that was continuously swept with cold nitrogen gas. This nitrogen gas was cooled by passing it through a copper coil immersed in liquid nitrogen. Temperatures as low as -250° F can be attained in this manner. To attain temperatures as low as -320° F, liquid nitrogen was sprayed directly on the

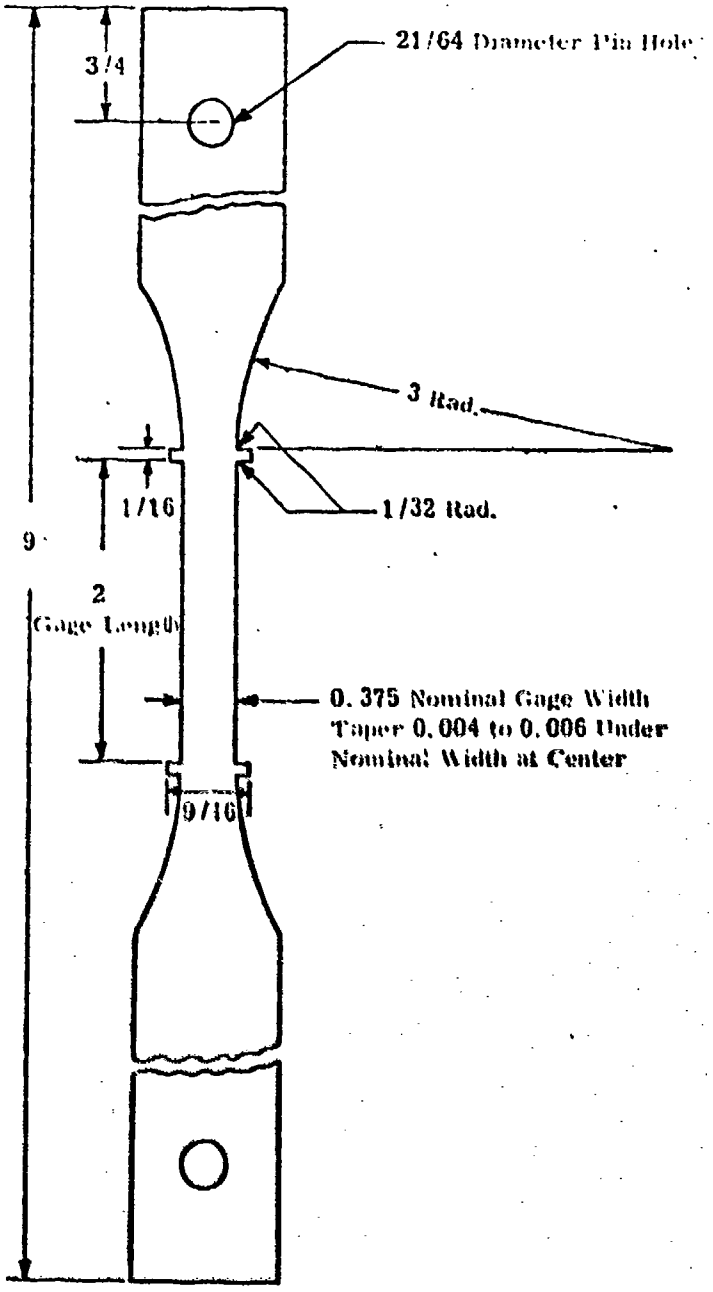

Figure 3. Sheet Tensile Specimen

specimen along its gage length. For the elevated-temperature work, the standard tensile specimens were resistance heated by current supplied from a high-current step-down transformer controlled by a saturable reactor. The fatigue-cracked specimens were heated in the temperature range from room temperature to above 1500° F with two focused radiant-heating fixtures. Both surfaces of the specimen were uniformly flooded with radiant energy from G. E. Type 500 T3/CL tubular infrared lamps with clear quartz envelopes. The putput from the three lamps in each reflector was concentrated upon the surface of the specimen by a focused reflector in the form of a half section of an elliptic cylinder.

Temperature control was effected by means of a 36-gage chromel-alumel thermocouple flash welded to the gage section of the specimen and connected to a temperature controller working in conjunction with the radiant lamps or resistance heater for the elevated temperatures, and with a solonoid valve in the nitrogen-gas line for the low-temperature work.

A criterion of crack-propagation determined for all of the materials was net fracture stress, which is identical with "sharp notch strength." Net fracture stress, as used in this report, is defined as the maximum load divided by the original net supporting area through the crack plane. For those refractory metals and alloys in which a brittle-ductile transition range was found, values of K_c, a fracture-toughness parameter, were calculated for the "brittleness" temperature ranges. These K_c values were generally "best estimates" based on calculations in which the original fatigue-crack length, $2a_o$, rather than critical crack length was used. Because of the nature of these materials, it was difficult (if not impossible) to discriminate between zones of shear fracture and flat tensile fracture in the fracture surfaces of the specimens. Therefore, the method for estimation of critical crack length by the percentage of shear in the fracture (1) could not be used. The compliance gage, with which direct measurement of slow crack extension can be made, was, unfortunately, not developed until later in the program, and only limited use of the gage was made.

Standard tensile properties—0.2%-offset yield strength, ultimate tensile strength, percent elongation in 2 in., and percent reduction of area at fracture—were obtained for each material for comparison with the crack-propagation properties.

V. RESULTS AND DISCUSSION

The following sub-sections contain graphical presentations of the data obtained in the several phases of the experimental work. The first two sub-sections show the comparative standard tensile properties and crack-propagation properties of the super-alloys and refractory metals evaluated in the program. The remaining sub-sections are concerned with the experiments on strain-aging of steels and the use of the compliance gage for crack-toughness determinations. It should again be noted that crack-propagation specimens used in obtain these data were 1.5 in. wide with a central transverse slot of about 0.4 in. which terminates in natural cracks produced by cyclic axial stressing. The over-all crack length, including the slots, was nominally 0.5 in. Each data point in the graphs for the super alloys and refractory metals represents from one to four individual determinations depending upon the material and the temperature. The exact number of specimens used for each condition can be determined from the data tables in Appendix A.

In the evaluations of the super-alloys and refractory metals, a loading rate of approximately 100 lb/sec was used in the determination of tensile and crack-propagation properties.

The experimental data for all of the materials are given in tabular form in Appendix A.

A. Super Alloys

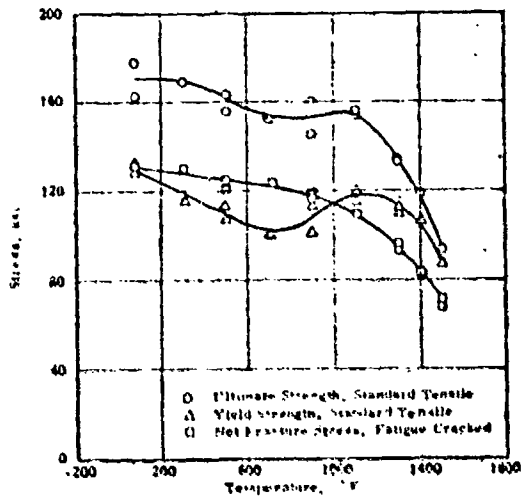

Figure 4. Effect of temperature on the standard tensile properties and net fracture stress of longitudinal specimens of aged Inconel-X.

The effects of temperature on the tensile-strength properties and net-fracture stress of aged Inconel-X are shown in Figure 4 and are presented in Tables 4 and 5 in Appendix A. Additional aging, occurring at temperatures above 900° F, evidently caused an increase in yield strength, with a maximum at about 1150° F. At temperatures above 1000° F, the net-fracture stress was below the yield strength, and at temperatures of 1400° F and 1500° F, the fractures of the fatigue-cracked specimens had flat tensile surfaces.

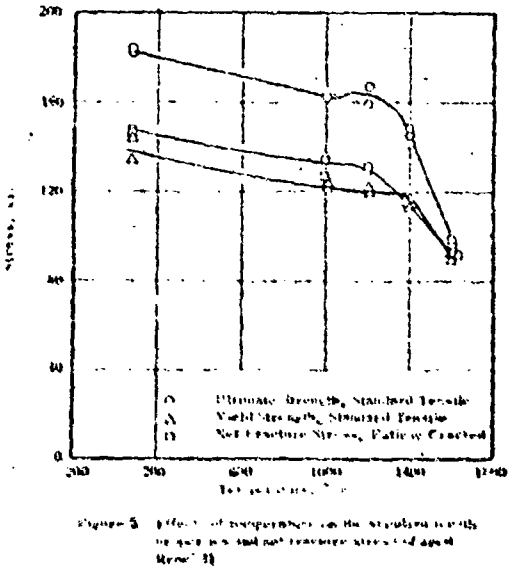

Figure 5 shows the effect of temperature on the tensile properties and net fracture stress of Rene' 41, nickel-base alloy, aged at 1400° F for 16 hr. These data are also presented in Tables 6 and 7 in Appendix A. The net fracture stress of the Rene' 41 was above the yield strength at all temperatures up to 1200° F. Above 1200° F, the net fracture stress was equivalent to the yield strength.

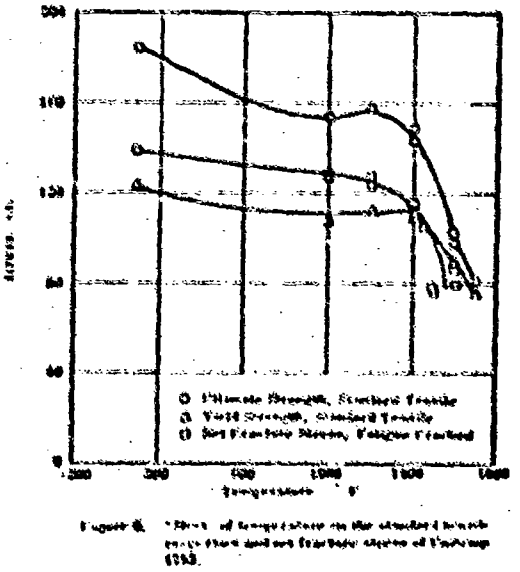

Figure 6 shows the effect of temperature from 75° F to 1700° F on the standard tensile properties and net fracture stress of aged

Unitemp 1753. These data are also given in Tables 8 and 9 in Append. A. The plateau in yield strength out to 1400° F is presumably a result of additional aging that occurred at temperatures from about 1200° F to 1400° F. The net-fracture stress tended to fall below the yield strength at temperatures above 1400° F. The flat tensile fracture surfaces of the fatigue-cracked specimens fractured at temperatures from 1400° F to 1600° F are also indicative of a marked tendency toward brittleness in this temperature range.

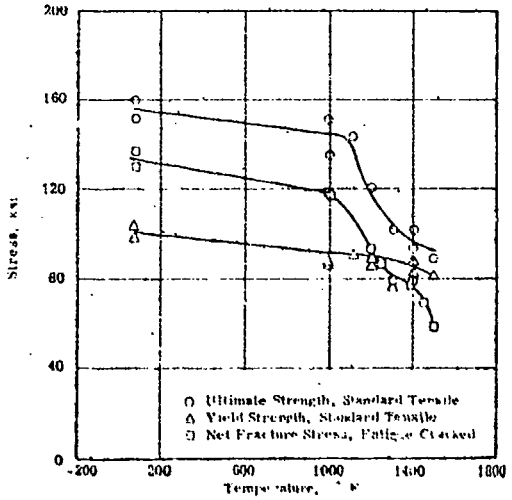

Figure 7. Effect of temperature on the standard tensile properties and net fracture stress of aged Nimonic 90.

In Figure 7, the effects of temperature on the standard tensile properties and net-fracture stress of aged Nimonic 90 are shown. These properties are also given in Tables 10 and 11 in Appendix A. The net-fracture stress is intermediate between the ultimate strength and yield strength at temperatures from 75° F to 1200° F, but beginning at about 1000° F, there is a decided decrease in crack toughness with increasing temperature. At temperatures above 1200° F, the fracture surfaces of the fatigue-cracked specimens were all flat tensile. There is little evidence, such as was shown by the Inconel-X, Rene' 41, and Unitemp 1753 of additional aging of Nimonic 90 at the higher temperatures.

The reduction in fracture toughness of the nickel-base alloys at elevated temperatures, as manifested by the decrease in net fracture stress-yield strength ratio at temperatures above about 1100° F, is probably related to the decrease in tensile ductility at this same

temperature range. Reduction in the tensile ductility of these alloys at temperatures above 1100° F is well established.

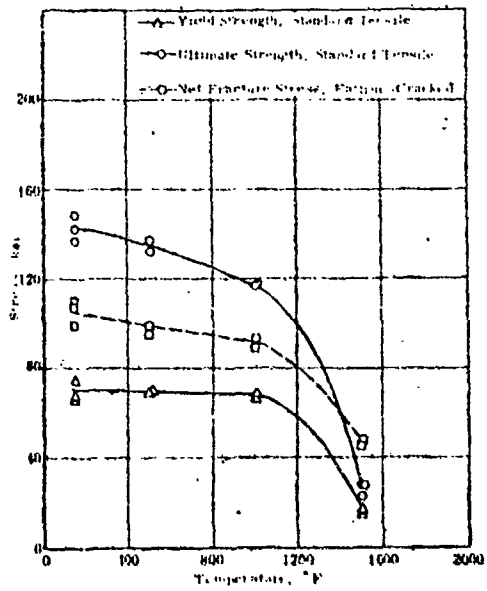

Figure 8 shows the effect of temperature on the properties of aged A-286 austenitic iron alloy. The properties are also presented in Tables 12 and 13 in Appendix A. Over the temperature range from 75° F to 1000° F, the net fracture stress of the A 286 was intermediate between the yield strength and ultimate strength. At 1500° F, the net fracture stress was considerably higher than the ultimate tensile strength. Thus, this austenitic iron-base alloy is reasonably notch-insensitive over the lower range of elevated temperatures and is quite notch-ductile at high temperatures.

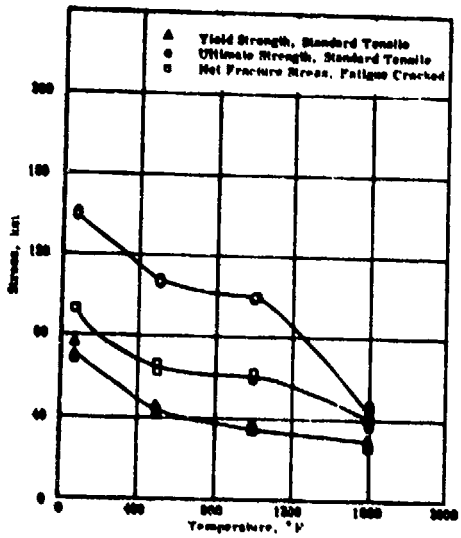

Figure 9. Effect of temperature on the tensile-strength properties and net fracture stress of annealed L 605 cobalt-base alloy sheet.

As shown in Figure 9,and in Tables 14 and 15 in Appendix A, within the range of temperatures from 75° F to 1600° F, the net-fracture stress of the L 605 was intermediate between the yield strength and ultimate strength; at 1600° F; the net fracture stress of the fatigue-cracked specimens and ultimate strength of the tensile specimens were essentially the same. This indicates that the L 605 is quite notch ductile over the entire temperature range investigated.

B. Refractory Metals

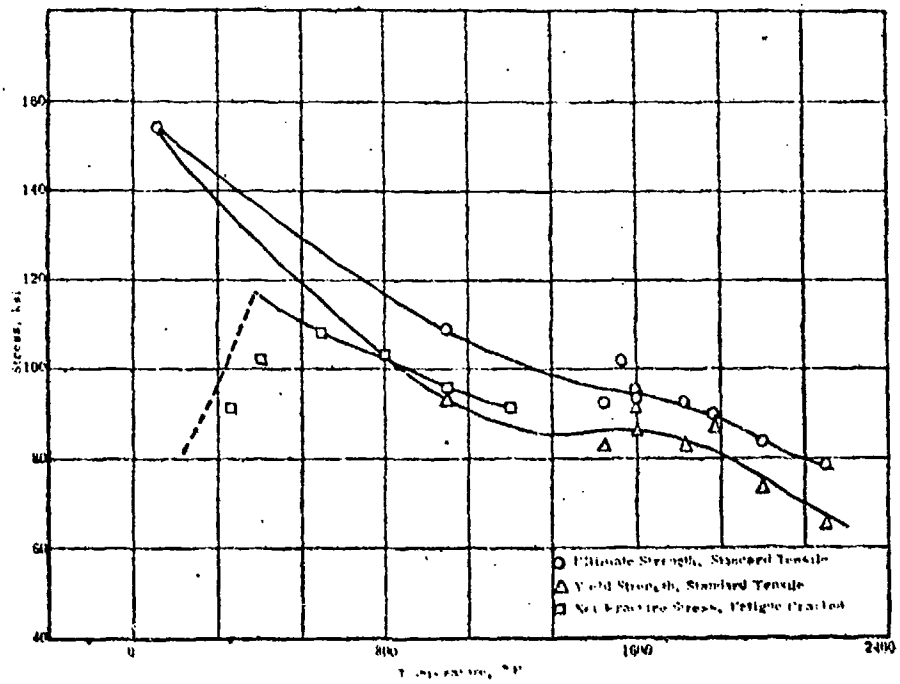

Figure 10 Ultimate strength, yield strength, net fracture stress of unalloyed annealed tungsten sheet as functions of temperature.

Figure 10 shows the tensile properties and net fracture stress of 0.040-in.-thick unalloyed tungsten sheet, prepared by the powder metallurgy method. These properties are also shown in Tables 16 and 17 in Appendix A. There is evidence of a slight tensile-strength maximum at 1600° F; this effect may be a manifestation of strain aging of the tungsten. The crack-propagation properties of the 0.040-in. tungsten sheet were investigated in the temperature range 300° F to 1200° F.

It was originally intended to extend the central notch to 0.5 in. in the tungsten sheet specimens by the same fatigue method used in the preparation of the crack-propagation specimens of all the other materials evaluated in this program. Extension of the crack in this manner, however, did not prove feasible; the central notched specimens did not show visible evidence of fatigue cracks after prolonged cyclic stressing both at room temperature and at 1000° F. Since there was a high incidence of specimen breakage in handling and mounting the tungsten specimens in the attempt to produce fatigue cracks, it was decided to abandon further attempts at producing fatigue cracks and

to machine the notch ends to as small a root radius as possible. The ends of the notch were impact ground to a radius of about 0.0005 in.

The specimens were then fractured in tension at temperatures from 300° F to 1200° F, the temperature range being limited by the small number of crack-propagation specimens available. In the evaluations at 300° F and 400° F the specimens fractured at the supporting pin holes rather than at the central notch. Each value shown in the stress level in the region of the central notch at the maximum load attained. It can be stated that the net-fracture stress was at least as large as the values shown. The fracture appearance at 600° F and higher was full shear, while the fracture appearance of the specimens that fractured at the pin holes indicated a purely brittle fracture. Since the portion of the specimen in the grip was at only a slightly lower temperature than the specimen gage section we may conclude that the brittle ductile transition temperature is in the region 300° F to 500° F. This is indicated by the dashed line in Figure 10. Again, no attempt was made to calculate K_c values, since the net fracture stress of the tungsten was generally equivalent to, or exceeded the yield strength over the range of temperatures investigated, and the K_c parameter is not of great significance under these conditions.

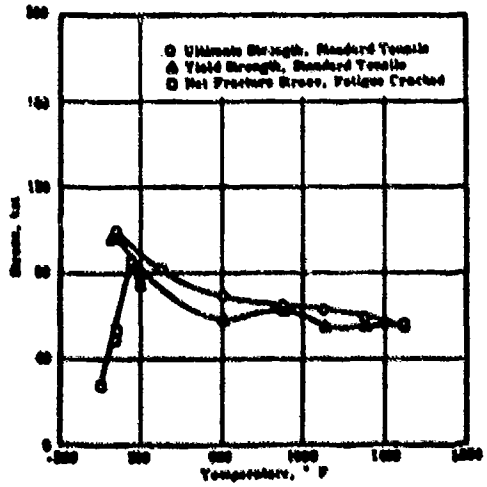

Figure 11. Effect of temperature on the standard tensile properties and net fracture stress of annealed longitudinal specimens of unalloyed molybdenum sheet.

Figure 11 shows the effect of temperature from 30° F to 1500° F on the standard tensile properties and from 0° F to 300° F on the net fracture strength of stress-relieved unalloyed molybdenum sheet.

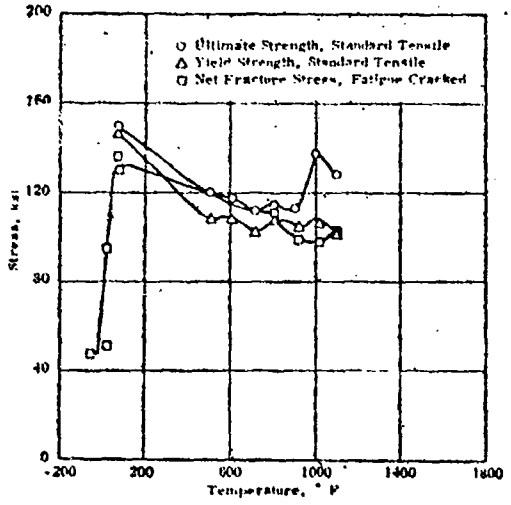

Figure 13. Effect of temperature on the standard tensile properties and net fracture stress of annealed longitudinal sheet specimens, 0.060 in. thick, of TZM molybdenum alloy.

Figure 13 shows the effect of temperature on the standard tensile properties and fracture properties of stress-relieved TZM molybdenum-alloy sheet. These properties are also given in Tables 22 and 23 in Appendix A. The transition temperature on the basis of net fracture strength is 65° F. The ultimate strength shows a significant "peak" at 1000° F, with a corresponding drop in net fracture stress at that temperatures. These effects are similar to those found in low-alloy steels (4) at a somewhat lower temperature—about 350° F. It is believed that the "strengthening" and reduced notch ductility noted in these cases are associated with strain-aging, that is, the "pinning atmospheres" of interstitials around dislocations.

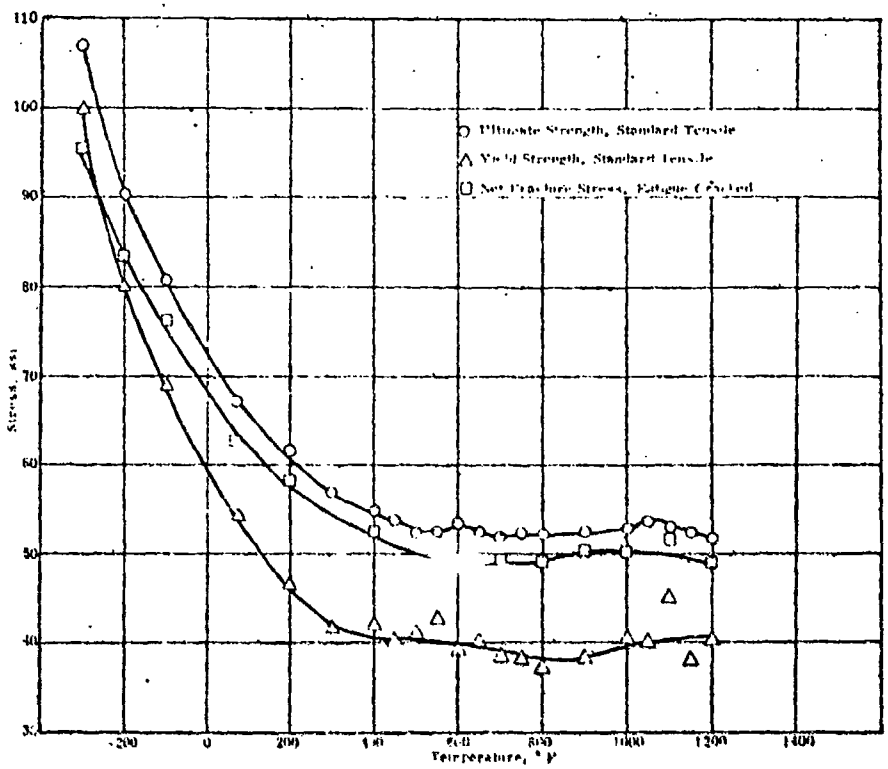

Figure 14. Ultimate strength, yield strength, and net fracture stress of cold-rolled and stress-relieved 0.050 in. thick D-14 columbium alloy sheet as functions of temperature.

Figure 14 shows the tensile properties and net fracture stress of cold-rolled and stress-relieved D-14 columbium alloy sheet. These properties are also given in Tables 24 and 25 in Appendix A. Since the D-14 was ductile down to the lowest temperature used in these evaluations, -320° F, no measurements of slow crack extension by means of the compliance gage were made, and no values of the fracture-toughness parameter, K_c, are reported. The K_c parameter is not of great significance when general yielding occurs across the supporting section of the crack-propagation specimen.

Whether or not the small relative maxima in the tensile strength properties at temperatures of about 600° F and 1100° F, as shown in Figure 14, represent actual strain-aging peaks is debatable. For example, the lower-temperature (600° F) peak represents a deviation of only 2.7% from the smooth curve; with specimens as small as those used here, non-uniformities in the material might be sufficient to produce a deviation of this magnitude. On the other hand the elevated-temperature values plotted represent average values obtained for from

two to four determinations at each temperature with specimens selected randomly from the sample sheet. Furthermore, in the temperature range of both the 600° F and 1100° F maxima there is a rather wide scatter in the yield strength. Willhelm (2) has reported wide scatter in tensile properties in the region of a strain aging peak in columbium. Serration of the stress-strain curve appeared at the higher-temperature peak but not at the lower-temperature peak. Both yield-strength scatter and serrated plastic stress-strain curves are often manifestations of strain aging. In any event such effects as these for D-14 are not of the magnitude as those reported elsewhere for unalloyed columbium and for other columbium alloys (2, 3). Apparently, the interstitial elements responsible for strain-aging phenomena in other columbium-base materials are not present in sufficient quantities to produce pronounced effects in D-14.

Although there is no evidence of a brittle-ductile transition at the lower-temperature end of the curve, the fact that the net fracture stress becomes lower than the yield strength at temperatures below -260° F indicates that the transition temperature may not be far below -300° F.

It may be concluded that the D-14 alloy is not subject to brittle fracture at ordinary strain rates at temperatures from -300° F to 1200° F; rather, failure by general yielding occurs, with specimens containing natural cracks (fatigue cracks), within this temperature range.

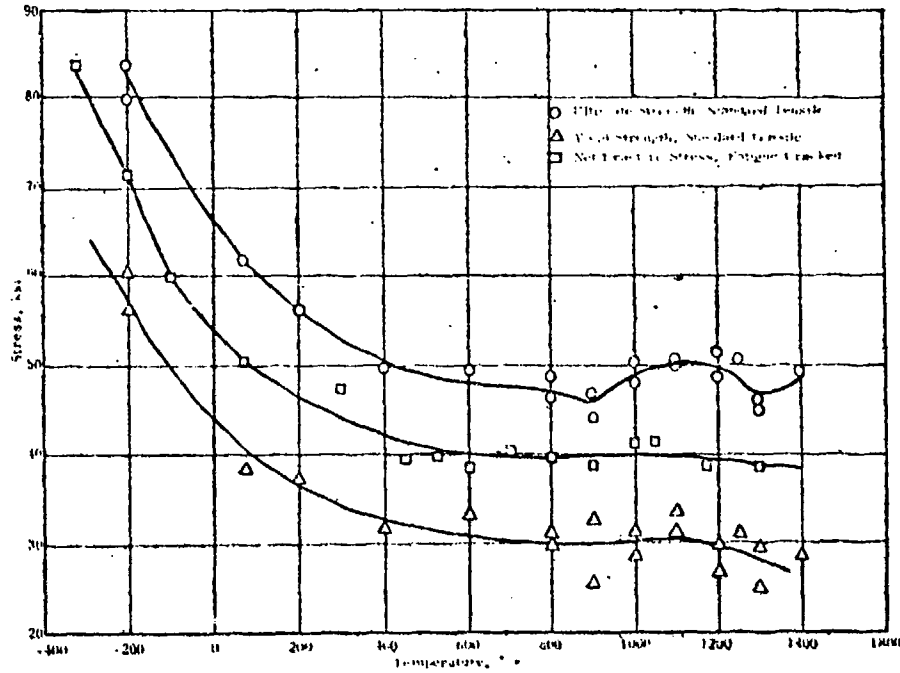

Figure 15. Ultimate strength, yield strength, and net fracture stress of stress-relieved FS-82 columbium alloy sheet as functions of temperature.

The tensile properties and net fracture stress of stress-relieved FS-82 columbium alloy sheet are shown as functions of temperature in Figure 15. These properties are also shown in Tables 26 and 27 in Appendix A. Since the FS-82 was ductile down to the lowest test temperature, -320° F, no measurements of slow crack extension by means of the compliance gage were made, and no values of the fracture-toughness parameter, K_c, are reported.

The relative maximum in the ultimate strength at about 900° F is evidence of strain aging in the FS-82. According to the data given by Wilcox and Huggins (3), a relative maximum in the ultimate strength of unalloyed columbium at this temperature and at the strain rate used here (about 10^{-3} sec $^{-1}$) can be attributed to interstitial nitrogen. Their data also predicts a second peak at a lower temperature due to interstitial oxygen. Since the oxygen content of the FS-82 was relatively large, a strain aging peak at a temperature below 900° F might be expected. Although this low-temperature peak did not occur in our data, there is evidence in Figure 15 that there may be another strain-aging peak at higher temperatures than those shown since the ultimate strength appears to increase again with increasing temperature after a slight drop at 1300° F. It may be that both the nitrogen- and oxygen-related strain-aging peaks occur at higher temperatures in the highly alloyed FS-82

sheet (containing over 34% tantalum) so that the peak actually observed is attributable to interstitial oxygen. As is evident in Figure 15, there is no significant effect on net fracture stress that could be associated with strain aging within the temperature range from -320° F to 1300° F.

C. Strain-Aging Effects in Steels

An investigation was made of the relative maximum in tensile strength and an apparently associated minimum in net fracture stress that often occur at temperatures of about 300° F to 400° F in low-alloy and carbon steels. These effects were noted in a prior research program conducted at Southern Research Institute (4). The relative tensile-strength maximum is thought to be a manifestation of the phenomenon of strain aging. Strain aging has been discussed extensively by Cottrell and Bilby (5)[2]. According to the strain-aging concept, there is an equilibrium atmosphere of interstitial elements around a dislocation in a metal. This atmosphere tends to increase the resolved shear stress necessary to cause the dislocation to move, i. e., tends to anchor the dislocation. Once the dislocation has broken away from the interstitial atmosphere the resolved shear stress required to move it decreases. If the rate of diffusion of the interstitial elements is increased, the atmosphere is able to travel with or catch up to the dislocation, tending to retard the motion of the dislocation and thus to strengthen the material. Thus the strengthening effect of strain aging is manifested when the temperature is in a range that allows the interstitials to diffuse at about the same rate that the dislocations are caused to move by an applied stress. At lower temperatures the inability of the interstitials to diffuse rapidly enough allows the dislocations to break away from the interstitial atmospheres under an applied stress. At higher temperatures the ability of the interstitials to diffuse more rapidly decreases their tendency to retard the motion of dislocations. On the basis of this explanation, the relative maximum should be markedly strain-rate sensitive. In particular, since diffusion is a time-rate process, a higher strain rate should decrease the ability of the atmospheres to catch up to the dislocations, and thus a corresponding decrease in the height of the maximum would be expected. Further, the temperature at which the maximum occurs would be expected to increase with increasing strain rate.

---

[2] In the article referred to, Cottrell and Bilby are mainly concerned with interstitial carbon, but similar effects have been attributed to interstitial nitrogen.

As a first step in this study, tensile-strength data were obtained on AISI 4130 steel at three radically different strain rates and over a temperature range of -100° F to 500° F. The source and composition of the 4130 steel are shown in Table 3. The three strain rates were 1×10^{-5} in. /in. /sec, 5×10^{-3} in. /in. /sec, and 0.5 in. /in. /sec. The tensile specimens were the same as those described in the specimen section of this report and were all taken with the sheet rolling direction along the long axis. The specimens were oil-quenched from 1570° F and then tempered at 400° F for 2 hours. The tensile data for the 1×10^{-5} in. /in. /sec strain rate are given in Table 28; the tensile data for the 5×10^{-3} in. /in. /sec strain rate are given in Table 29; and the tensile data for the 0.5 in. /in. /sec strain rate are given in Table 30. All of these tables appear in Appendix A.

In addition to the standard tensile data, data were obtained on the net fracture stress of centrally fatigue-cracked specimens of quenched and tempered 4130 at temperatures from -240° F to about 350° F or higher. The fatigue-cracked specimens were loaded at three different free crosshead travel rates which were the same as those used to produce the three different strain rates in the standard tensile specimens. Since "strain rate" is not an applicable term for fatigue-cracked specimens, average loading rates are reported for the three different crosshead travel rates. The loading rate comparable to each strain rate is given below:

Strain Rate	Comparable Loading Rate
1×10^{-5} in. /in. /sec	4 pounds/sec
5×10^{-3} in. /in. /sec	2×10^{3} pounds/sec
0.5 in. /in. /sec	2×10^{5} pounds/sec

These values were calculated from measurements of time to failure and maximum load and are therefore only average values.

The fracture-strength data at a loading rate of 4 pounds/sec are given in Table 31, the strength data at a loading rate of 2×10^{3} pounds/sec are given in Table 32; and the strength data at a loading rate of 2×10^{5} pounds/sec are given in Table 33. All of these tables appear in Appendix A. The tensile data and net fracture strength are presented graphically as functions of temperature for three different rates in Figures 16, 17, and 18.

Table 3

Source and Composition of AISI 4130 Steel

Heat No.	Manufacturer	As Received Condition	Gaseous Elements ppm			Chemical Composition % by Weight											
			O	N	H	C	P	S	Si	Mn	Cr	Ni	Mo	Co	Ti	Al	B	Fe
110013	Crucible Steel Company	Normalized Condition	65	120	4.4	0.33	0.12	0.020		0.48	0.84		0.16					Bal

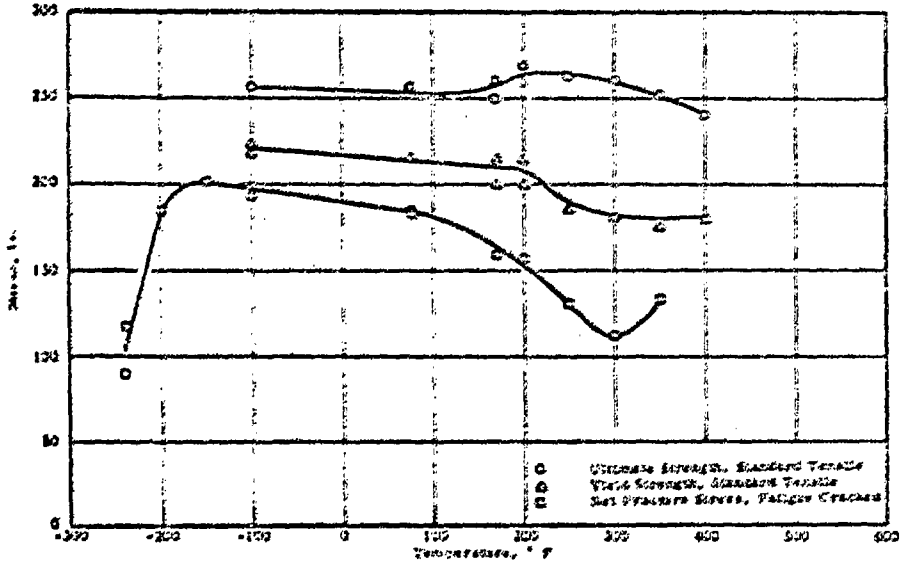

Figure 16. Effect of temperature on the standard tensile strength properties and fracture strength properties of quenched and tempered AISI 4130 sheet steel at a nominal strain rate of 1×10^{-3} in./in./sec.

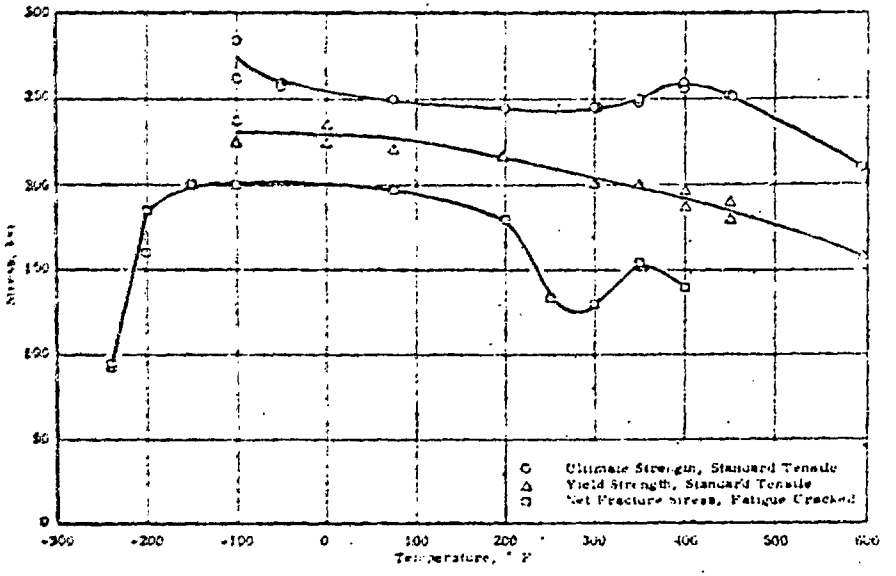

Figure 17. Effect of temperature on the standard tensile strength properties and fracture strength properties of quenched and tempered AISI 4130 sheet steel at a nominal strain rate of 5×10^{-3} in./in./sec.

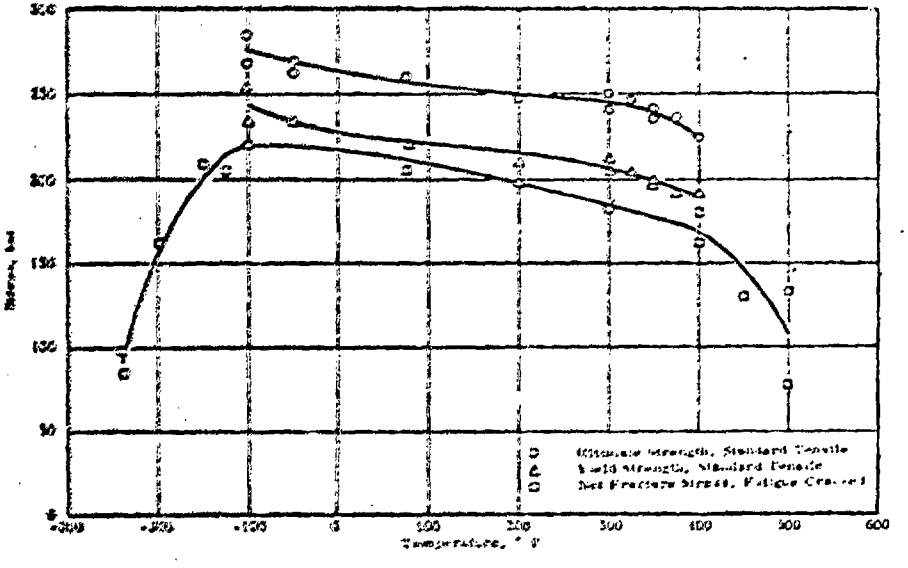

Figure 18. Effect of temperature on the standard tensile strength properties and fracture strength properties of quenched and tempered AISI 4130 sheet steel at a nominal strain rate of 0.5 in./in./sec.

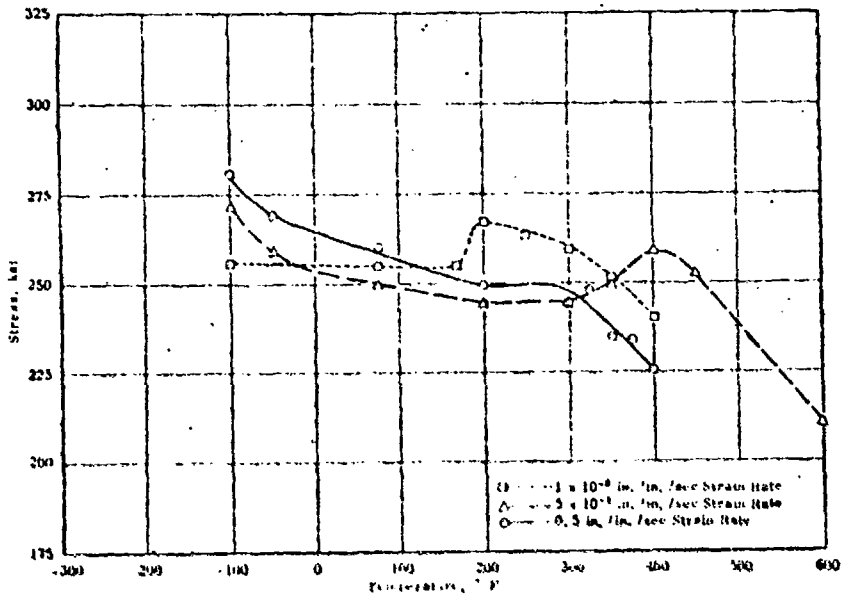

Figure 19. Ultimate tensile strength of tempered AISI 4130 steel sheet at different temperatures and three different strain rates.

Figure 19 compares the ultimate tensile strength of AISI 4130 steel sheet as a function of temperature for the three different strain rates. As expected, the relative maximum was quite strain-rate sensitive. The difference is most evident between the very high strain rate and the very low strain rate. At the low strain rate, the maximum occurs at about 200° F; for the very high strain rate, the maximum has essentially disappeared. At the intermediate strain rate, the maximum has shifted to temperature of about 400° F. Apparently, even at this moderately rapid strain rate, the material can still be strengthened by the diffusion of interstitial atmospheres to re-anchor dislocations, but the added mobility imparted by a higher temperature is required.

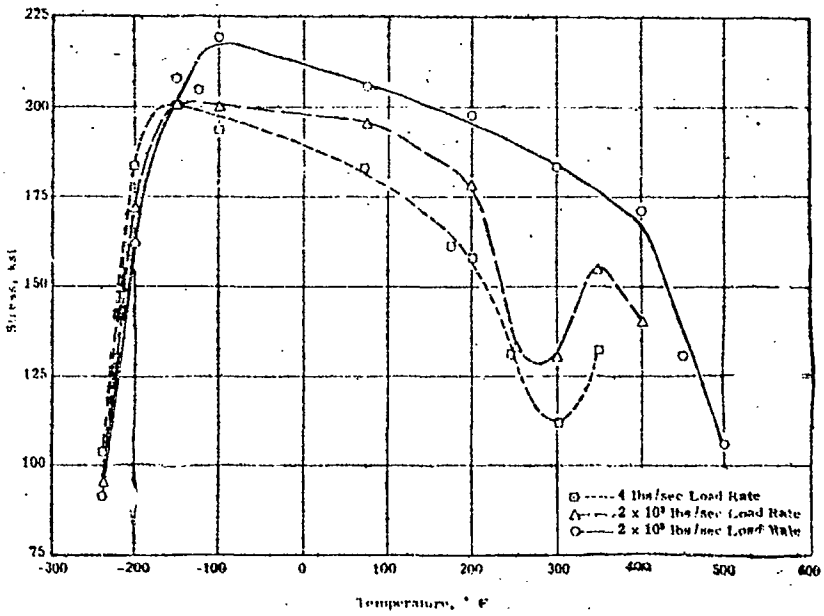

Figure 20. Net fracture stress of tempered AISI 4130 steel sheet at different temperatures and three different loading rates.

Figure 20 compares the net fracture stress of fatigue-cracked AISI 4130 steel sheet as a function of temperature for the three different loading rates. It is apparent that for the slow and intermediate loading rates there is a relative fracture-stress minimum in approximately the same temperature range where the maximum appeared in tensile-strength properties. At the very high loading rate there is virtually no relative minimum in the NFS-vs-temperature plot, corresponding to the lack of a strain-aging peak in the tensile data at the corresponding loading rate.

One of the molybdenum alloys, Mo 0.5Ti 0.08-Zr, exhibited a pronounced strain aging effect at about 100° F. It is interesting to note that this TZM alloy contained significantly more nitrogen (33 ppm) than the two other molybdenum sheet materials (about 15 ppm) in which there was only slight evidence of strain aging. The levels of the other interstitial gases, oxygen, and hydrogen, were essentially the same in all three of the molybdenum materials, and the carbon content of the TZM alloy was actually lower than that of both the unalloyed molybdenum and the Mo-0.5Ti alloy.

The nitrogen content of the AISI 4130 steel, as shown in Table 3 of this report, is also significantly high, being 120 ppm. It seems probable that the strain-aging effects observed both in the low-alloy steels and the refractory metals can be largely attributed to the nitrogen content of these materials.

In addition to the strain-aging effects, another effect of loading rate on fracture behavior is shown in Figure 20, namely, the effect on the brittle-ductile transition temperature. It has been suggested that the resistance to brittle fracture of tempered martensite should be affected only slightly by variations in loading rate, since the yield strength of this structure is increased only moderately by rather large increases in loading rate. As is shown in Figure 20, this is indeed true for the tempered martensitic structure of the AISI 4130 steel. An increase in loading rate of nearly five orders of magnitude resulted in a rather small increase in the net-fracture-stress transition temperature. At temperatures above the transition temperature, increasing the loading rate increased the net fracture stress.

In a further study of the effects of strain rate on the strain-aging phenomenon, the standard tensile properties and net fracture stress of hot-rolled AISI 1020 steel sheet were evaluated at temperatures in the range -320° F to 450° F. Two radically different strain rates were used. These strain rates and their comparable loading rates were almost identical with the maximum (0.5 in./in./sec) and minimum 1×10^{-5} in./in./sec) strain rates used in the evaluation of AISI 4130.

The type crack-propagation specimen (shown in Figure 2) used in the evaluation of AISI 1020 sheet permitted the use of the clip-on compliance gage. For calibration of the compliance gage, the length of the central-fatigue cracks in some of the crack-propagation specimens varied from 0.3 in. to 0.9 in. For the evaluation of the effects of loading rate on the fracture toughness of the 1020 steel, specimens with a fatigue crack length of 0.5 in. were used.

The tensile properties of AISI 1020 steel sheet at the high strain rate are given in Table 34; the fracture strength properties at the equivalent high loading rate are given in Table 35. The tensile properties of AISI 1020 steel sheet at the low strain rate are given in Table 36; the fracture strength properties at the equivalent low loading rate are given in Table 37. These tables appear in Appendix A. The 0.2%-offset yield strength, ultimate strength, and net fracture stress are given graphically as functions of temperature for the high and low crosshead-travel rates in Figures 21 and 22 respectively. In Figure 23 the ultimate tensile strength vs temperature curves at the two strain rates are plotted together, and in Figure 24 the net fracture stress vs temperature curves at the two different loading rates are plotted together.

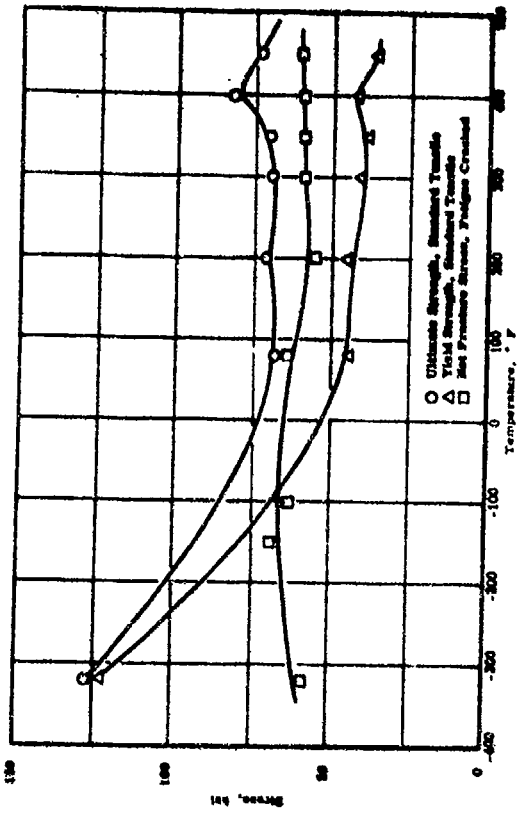

Figure 32. Effect of temperature on the standard tensile strength properties and fracture strength properties of hot-rolled ABS 1035 steel sheet at a nominal strain rate of 1×10^{-3} in./in./sec.

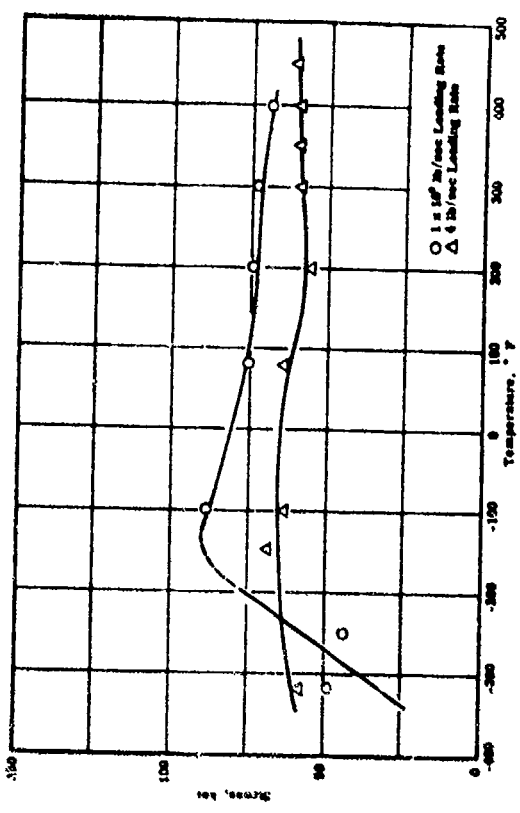

Figure 34. Net fracture stress of fatigue-cracked hot-rolled ABS 1035 steel sheet as a function of temperature at two different loading rates.

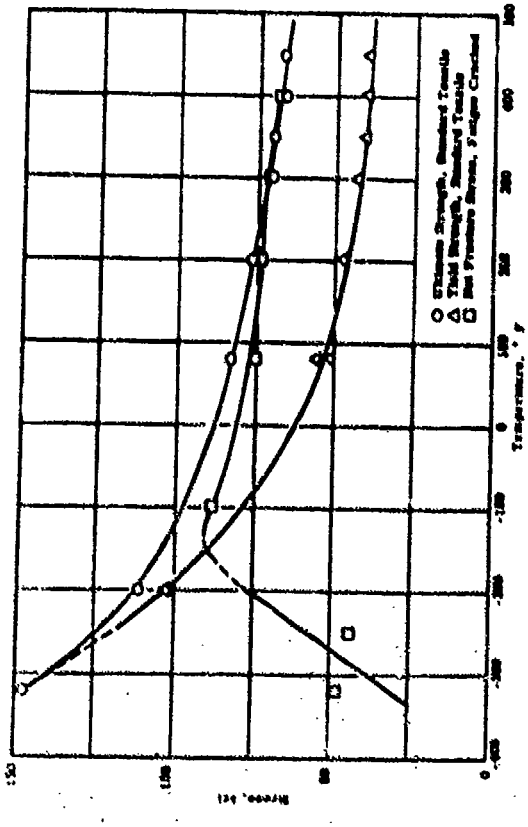

Figure 33. Effect of temperature on the standard tensile strength properties and fracture strength properties of hot-rolled ABS 1035 steel sheet at a nominal strain rate of 0.3 in./in./sec.

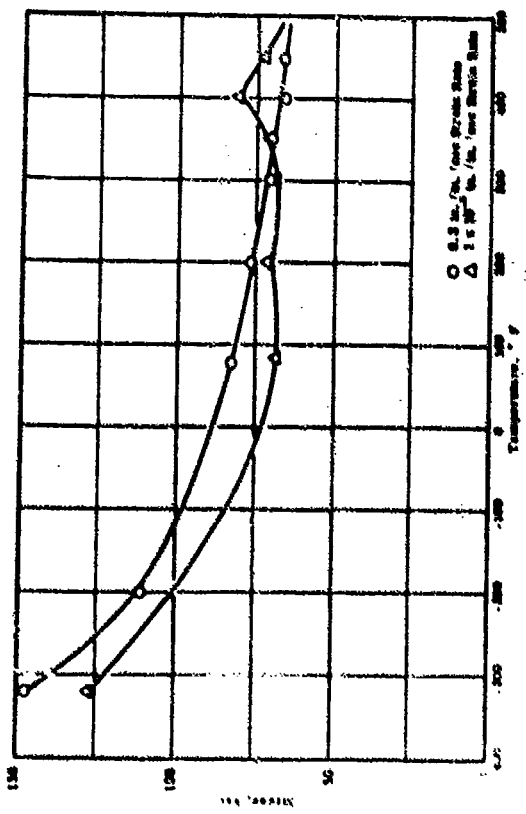

Figure 35. Dynamic tensile strength of hot-rolled ABS 1035 steel sheet as a function of temperature at two different strain rates.

In Figure 22, it is shown that the ultimate tensile strength has a relative maximum at about 400° F at the low strain rate. At the high strain rate this maximum has either disappeared or shifted to temperatures above those shown. This relative maximum is probably a result of strain aging in the material. Such strain-aging peaks are normally shifted to higher temperatures with increasing strain rates.

The strain-aging peak of AISI 1020 may be compared with that of tempered AISI 4130. For the strain rate of 1×10^{-3} in./in./sec, the strength peak of AISI 4130 occurs at around 200° F. In AISI 1020 steel, although there is slight evidence of a strengthening effect at 200° F, the main strengthening occurs at 400° F. It is thought that this difference in the temperature for the occurrence of strain aging in the two steels is attributable to the effects of structural differences between the steels--a tempered martensite in the 4130 and ferrite and fine pearlite in the 1020.

In Figure 21 it is seen that, at the high loading rate, there is a rather abrupt decrease in the net fracture stress of the 1020 below about -100° F. As shown in Figure 22, the net fracture stress of the 1020 at the slow loading rate is essentially the same over the entire temperature range from 450° F to -320° F. It is interesting that, for both loading rates, the net fracture stress became lower than the yield strength at approximately the same temperature, around -125° F to -150° F.

From these experiments with AISI 4130 steel, heat treated to a strength level of 250,000 psi, and with hot-rolled AISI 1020 steel, it seems that the occurrence of a net-fracture-stress minimum in the strain-aging temperature range (300° -400° F) is probably dependent on the structure of the material. The net-fracture-stress minimum was not observed in the relatively low strength 1020, but it was fairly pronounced in the higher strength 4130, whose structure was tempered martensite. This minimum has also been noted in other high-strength low-alloy steels (4).

VI. COMPLIANCE-GAGE EXPERIMENTS

This section of the report contains a description of the development and preliminary use of a special device for measuring slow crack growth in crack-propagation tests. The device described here, which is called a compliance gage, is a modification of the scheme originated at the U. S. Naval Research Laboratory by Krafft and Boyle (6, 7).

The compliance gage offers a means of determining critical crack length without the use of inks or stains, and it may be used over a wide temperature range.

Boyle (6) has described a method of measuring the mechanical compliance, which is the extension-load ratio, of a central notched or cracked sheet specimen and has demonstrated how this measurement of compliance can be used to give a reliable estimate of notch depth or of notch depth plus cracks extending from the notch roots. The method is based on the fact that the compliance of a centrally cracked sheet is a function of the length of the crack (more accurately a function of the projection of the length of the crack on the transverse axis). As a crack extends, the compliance increases (stress now being taken as the gross stress calculated from the dimensions of the uncracked specimen) finally increasing without bounds as the crack reaches the edges of the specimen. As tension is applied to a centrally cracked sheet specimen, the extension of the specimen increases approximately linearly with applied gross stress until a stress level is reached at which crack extension occurs. As the crack extends, the slope of the load-extension curve decreases (load as ordinate) because of the increased compliance of the specimen. When the stress reaches an appropriate level, the specimen fails (the crack propagates rapidly across the remaining specimen width). In order for the calculation of critical crack length to be valid, it must be assumed that the compliance calculated from the slope of a line drawn from the origin of the load-extension curve to the point of discontinuity is the same as the compliance of a specimen that contains an original crack the same length as the critical crack. Boyle demonstrated that this assumption is valid.

Boyle used an extensometer arrangement that measures the displacement between two points on the central axis of the specimen—one below and one above the crack. For ordinary tensile determinations Southern Research Institute has developed and used extensively a simple extensometer that clips on to lugs machined at the specimen gage points. Since this extensometer has been employed successfully in a variety of atmospheres and at temperatures from -320° F to 3000° F, it was considered desirable to see if the extensometer might be employed in the measurement of compliance for critical crack-length determination. The advantages of being able to measure critical crack lengths in inert atmospheres and at temperatures from -320° F to 3000° F are obvious. A diagram of the extensometer arrangement in place on a centrally cracked specimen was shown in Figure 2, in a previous section of the report.

Irwin has indicated that compliance, measured away from the specimen central axis, is not as large as compliance measured on the axis (8). Accordingly, it was decided to determine whether the sensitivity obtained in measuring compliance of the specimen edges was sufficient for determinations of slow crack extension. First, an analysis was carried out, based on Irwin's modification of Westergaard's equation (9), for compliance as measured at the edges of the specimen. Figure 25 shows the plot of compliance as a function of crack length from the derived equation:

$$\frac{Ev}{\sigma w} = \frac{2}{\pi} \sinh^{-1} \left[\frac{\sinh \frac{\pi y}{w}}{\cos \frac{\pi a}{w}} \right] - \frac{y}{w} \frac{(1+\nu)}{\sqrt{1 - \frac{\sin^2 \frac{\pi a}{w}}{\cosh^2 \frac{\pi y}{w}}}} + \frac{\nu y}{w}$$

The units are those used by Irwin and Boyle (6, 9): a is one-half of the crack length, w is the specimen width, v is one-half of the specimen extension, σ is the gross stress calculated from the dimensions of the uncracked specimen, and E is Young's modulus. Appendix B shows the derivation of the equation that adapts the Irwin-Westergaard equation for compliance at the edges of the specimen. A compliance vs crack-length calibration curve was prepared in much the same manner as that by Boyle (6); specimens were prepared having different original crack lengths; the compliance of each specimen was measured; then the specimens were fractured and the actual starting crack length measured. The compliance of the specimens was measured under two different conditions: at very small applied stresses and at stresses 70 - 80% of that required to produce crack extension.

The compliances measured at low stress gave much better agreement with the theoretical curve than the compliances measured at the higher stress. This, of course, is to be expected since the stress analysis is valid only for very small strains. The compliances at low stress are plotted along with the theoretical curve in Figure 25. Compliances at the higher stress level are plotted as functions of crack-length parameter $\pi a/w$ in Figure 26. The difference in compliance values for these two different methods of measurement demonstrates that the "elastic region" of a load-extension curve for a central cracked specimen is not really linear but curved. One may, then, speak of two distinct compliances: one the limit of compliance as stress approaches zero (which is compliance described in the stress analysis), and the other a practical compliance taken as the average compliance over the so-called elastic region.

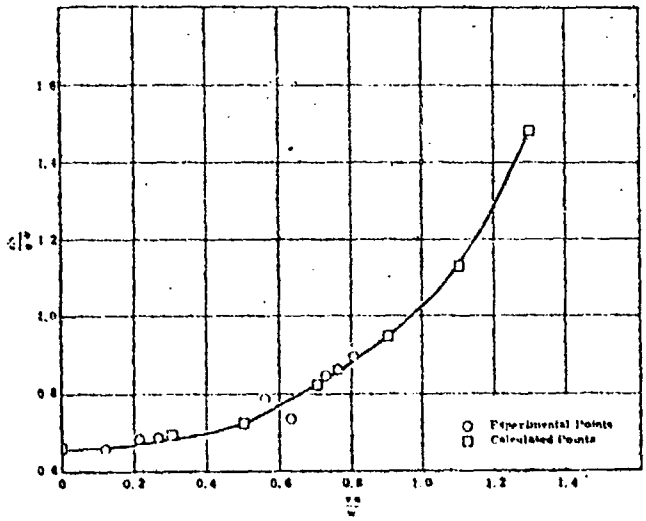

Figure 25 Compliance as a function of crack length curve derived from the Irwin-Westergaard equation. Also shown are experimental compliances measured at low stress levels.

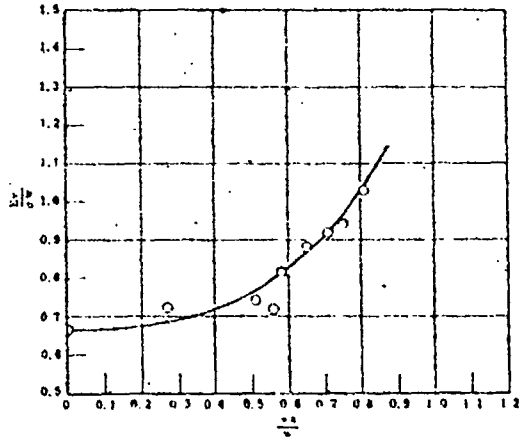

Figure 26 Compliance as a function of crack length calibration curve. Compliance measurements made at 70-80% of stress required to cause crack extension.

Figure 25 is the curve that was used in actual practice for the determination of critical crack length. The curve shown is not well defined at or below $\pi a/w$ values of 0.55, but for the usual crack-propagation specimens the original crack length gives a $\pi a/w$ value of about 0.52 so that the main concern is with $\pi a/w$ values greater than 0.52. Hot-rolled AISI 1020 steel sheet was used for determination of the calibration. The determinations were made in air at room temperature. The calibration curve should be valid for other materials and at other temperatures. All that is required is that Young's modulus be known for the material at the desired temperature.

Experiments with the compliance gage were made to determine the effectiveness of the gage in following slow crack extension at several temperatures and to determine the reproducibility of the fracture-toughness values obtained at a single temperature. Specimens for these experiments were prepared from two high-strength steels—300 M and AISI 4340—both of which have quite limited ductility over a rather wide temperature range above the brittle-ductile transition when they are heat treated to a high nominal strength level. It seemed probable that within this temperature range it would be possible to select a particular temperature at which sufficient slow crack growth would occur for a reasonable assessment of the reproducibility of the compliance-gage measurements. The experiments are described in two of the following sections, one section covering the 300 M and the other covering the AISI 4340.

A third section describes some preliminary experiments, made with sheet samples of 7075-T6 aluminum alloy, to evaluate the use of the compliance gage for determining the plane-strain fracture-toughness, K_{Ic}. The potential use for the compliance gage has been discussed by Krafft and Boyle (10), and this general method for the K_{Ic} determination has been called the "crack pop-in" method.

A. 300 M

Standard tensile specimens and crack-propagation specimens were prepared from 0.080-in.-thick 300 M sheet. The crack-propagation specimens were 1 1/2 in. in width and had machined lugs at the 2-in. gage points. Transverse saw-cuts were made in the center of the gage section. Most of the saw-cuts were initially about 0.4 in. long and were extended by cyclic stressing to an over-all crack length of about 0.5 in. In a few of the specimens, the saw-cut lengths were varied, and these cuts were extended by fatiguing to final crack lengths of from 0.60 to 0.93 in. These specimens were used as calibration standards to check the original calibration curve obtained with the use of AISI 1020 steel. All of the specimens were heat treated as follows: austenitized at 1600° F for 30 min, oil quenched; tempered twice at 600° F for 2 hr. The 300 M calibration data conformed very closely to the previously obtained calibration for AISI 1020 and to the theoretical compliance curve derived analytically, as is shown in Figure 27.

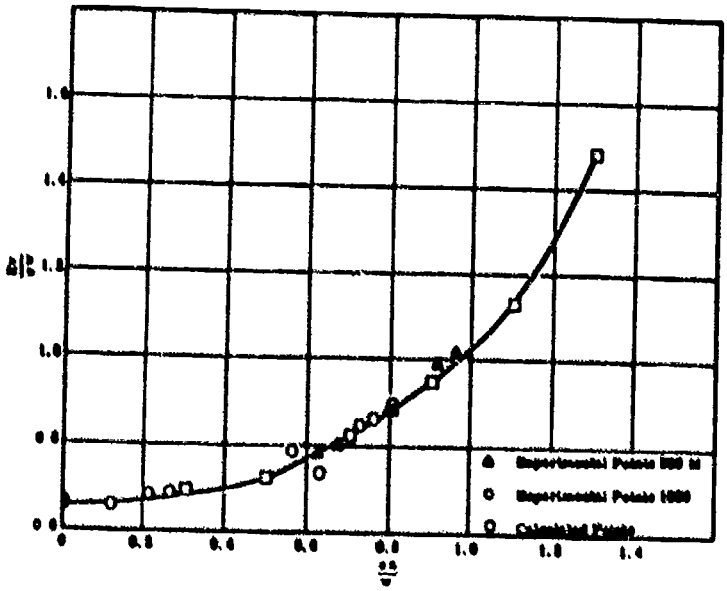

Figure 27. Compliance as a function of crack length curve derived from the Irwin-Westergaard equation. Also shown are experimental compliances measured at two stress levels for specimens of AISI 1020 and 300 M steels.

The remaining 300 M crack-propagation specimens, containing fatigue cracks of nominally 0.5 in. in length, were fractured at various temperatures from 75° F to 800° F to determine the effect of temperature on slow crack growth and the ability of the compliance gage to measure slow crack growth reproducibly. It was found that, although an appreciable amount of slow crack growth occurred at 75° F and 200° F, the cracks grew to considerably greater lengths at 400° F. Again, at 600° F and 800° F, generally less slow crack growth occurred than at 400° F. Therefore, a number of samples were run at 400° F as a reproducibility check on the compliance measurements. Standard tensile properties of the 300 M were also obtained at these same temperatures, since yield strength and elastic modulus are needed in the calculation of the fracture-toughness parameter, Kc. The standard tensile properties are shown in Table 39, and the crack propagation properties are shown in Table 40. Both of these tables appear in Appendix A. Both the standard tensile properties and crack-propagation properties are plotted as functions of temperature in Figure 28. It is interesting that the greatest amount of slow crack growth (largest critical crack length) occurs at the same temperature (400° F) at which there is a minimum in net fracture stress and a maximum ultimate tensile strength. Since the combination of lowered fracture stress and increased critical crack length tend to have a compensating effect, there is little change in the fracture-toughness parameter, K_c, in this region. Apparently, the increased amount of slow crack growth may be associated with a "low-energy shear" mechanism, which in turn accounts for the lowered net fracture stress in this temperature range.

Values of K_c at 400° F for 300 M varied from 88.4 to 132 ksi $\sqrt{\text{in.}}$; for five of the seven determinations, the values were within about ±15% of the average for the group—110 ksi $\sqrt{\text{in.}}$

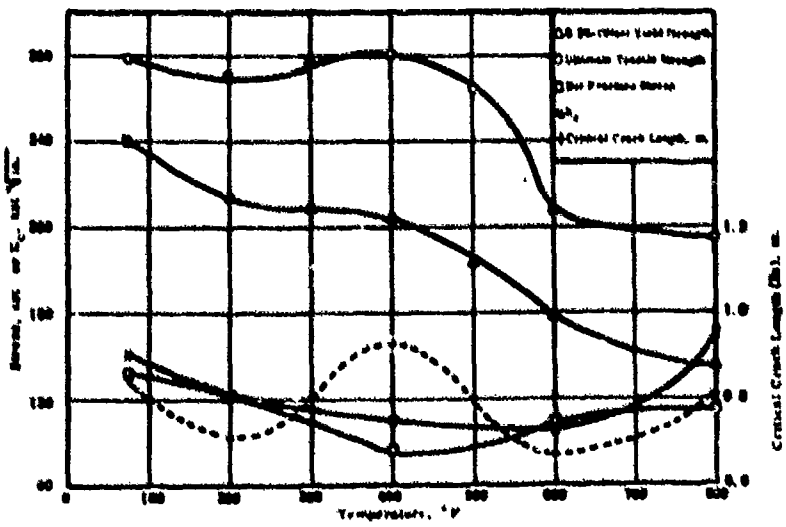

Figure 28. Effect of temperature on the standard tensile properties and crack-propagation properties of 300 M steel heat treated to 260 ksi nominal yield strength level

B. AISI 4340

Several standard tensile specimens and crack-propagation specimens were prepared from 0.064-in. thick AISI 4340 sheet. The 4340 fatigue-cracked specimens all had nominal crack lengths of 0.5 in. The specimens were austenitized at 1600° F for 30 min, oil quenched, and then tempered twice at 400° F for 2 hr. The standard tensile properties and crack-propagation properties were determined at 350° F, at which temperature a minimum in net fracture stress was known to occur for 4340 heat treated to this strength level. These properties are shown in Tables 40 and 40 in Appendix A. As was found for the 300 M, the 4340 sheet underwent considerable slow crack growth before fracturing at elevated temperature. Values of K_c for the 4340 ranged from 219 to 274 ksi $\sqrt{\text{in.}}$ with an average of 250 ksi $\sqrt{\text{in.}}$ for the five determinations (See Table 41 Appendix A). The fact that the toughness of the 4340 was apparently much greater than that of the 300 M for the same tensile strength level (280 ksi) is probably partly attributable to the greater thickness of the 300 M samples—0.080 in. as opposed to 0.064 in. for the 4340—since toughness is known to decrease with increasing sheet thickness. In any event, the toughness of the 4340 is surprisingly high (250 ksi $\sqrt{\text{in.}}$) for conditions under which the net fracture stress is only about 70% of the yield strength.

Experiments with two additional fatigue-cracked specimens of 4340 lend confirmation to the accuracy of crack-length determination with the compliance gage. In these experiments the samples were loaded in tension at 350° F until the compliance curve indicated a significant amount of slow crack extension had occurred, and then the loading was discontinued. The samples were then held in a muffle furnace at 400° F for several hours to heat-tint the surfaces of the cracks. The samples were then fractured, at room temperature, and the lengths of the heat-tinted fracture surfaces were measured. These measured values of crack length are consistent with the crack lengths calculated from the compliance data as is shown in the following tabulation:

Initial Fatigue Crack Length ($2a_o$)	Measured Extended Crack Length (Heat-Tint)	Calculated Extended Crack Length (Compliance)
0.50	0.78	0.81
0.54	0.71	0.73

C. 7075-T6, K_{Ic} Experiments

Another potential use for the compliance gage in fracture-toughness determinations has been reported by Krafft and Boyle (10). These investigators found that coincident with the audible "clicks" that occur at rather high stresses in crack-propagation specimens, immediately prior to measurable slow-crack extension, there was a small, sudden displacement indicated by the compliance gage. It was thought that this displacement occurred as the initial sharp notch or fatigue crack "popped-in" to a more stable crack front for slow growth. Assuming that the material had sufficient toughness, some slow crack extension would then occur prior to fracture. During this latter period, the behavior of the crack would be governed by the plane-stress crack extension force, G_c, and the plane-stress intensity parameter, K_c. However, it seemed probable that the crack "pop-in" behavior could correlate with the plane-strain parameter, G_{Ic}, since crack pop-in occurred before the development of a plastic zone at the crack tip. If such a correlation could be shown, the crack pop-in stress could be used to calculate a G-value that would be a good approximation of G_{Ic} for the material.

Krafft and Boyle showed that for 7075-T6 aluminum the "G_{nc}" values, calculated from pop-in stress obtained with the compliance-gage on sheet specimens up to 8 in. wide and containing "internal" sharp notches, were very close to the values for K_{Ic} obtained by means of circumferentially-notched bar specimens of 7075-T6.

Some experiments were conducted in the latter part of this program to determine whether crack pop-in could be detected with the SRI compliance gage attached to the edges of specimens of ordinary size. In the first experiments, fatigue-cracked specimens identical with that shown in Figure 2 were prepared from 0.090-in.-thick 7075-T6 sheet. These specimens were loaded to failure in a Tinius Olsen tensile machine fitted with a strain-gage load cell and with the compliance gage positioned at the 2 in. gage points on the specimen-edge lugs. From the load-deflection curve, traced on an X-Y recorder, the load at crack pop-in was obtained from the discontinuity in the load-displacement curve. The gross stress, representing this load value, was then used to calculate the "G_{nc}" by the following relationship:

$$G_{nc} = \frac{\sigma^2 W}{E} \tan \frac{\pi a_o}{W}$$

In this equation, a_o is the initial half crack-length or half notch-depth. By means of the relationship between G and K, a corresponding value

for the stress intensity parameter K_{nc} was calculated as follows:

$$K_{nc}^2 = \frac{E}{(1 - \nu^2)} G_{nc}, \text{ where } \nu = \text{Poisson's ratio.}$$

Values for G_{nc}, as determined with the 7075-T6 fatigue-cracked specimens, averaged about 65 lb/in., which is extremely low compared with the value of about 145 lb/in. reported by Krafft and Boyle for K_{Ic} determined with circumferentially-notched bars of 7075-T6.

It was decided to run some crack pop-in experiments with specimens containing internal notches ("shear cracks") rather than natural fatigue cracks. This decision was predicated on the idea that the plane-strain toughness may be more clearly manifested by a crack pop-in event that includes the development of a crack from a high stress-concentration. The specimens used in these experiments were similar to those in the prior pop-in experiments, except that they contained, instead of fatigue cracks, a transverse shear punch, or "shear crack," about 0.43 in. in length. The preparation of the shear-cracked specimens has been described in reports of a previous contract for the Bureau of Naval Weapons (4). The feature of this specimen believed to be important to the experiments described here is that the initial notch "front" is convex. Therefore, when pop-in occurs in a shear-cracked specimen there is a very large change in this front, and it would be expected that a rather large deflection would be recorded. Several shear-cracked specimens of the 7075-T6 were loaded in the Tinius Olsen machine by the same procedure as has been described for the fatigue-cracked specimens. A typical load-deflection curve for a shear-cracked specimen is shown in Figure 29. Crack pop-in for this specimen occurred at a load of 6280 lb, as is shown by the discontinuity in the load-deflection curve at that point. Beyond the pop-in point, slow crack extension is evidenced by the changing slope, and fracture occurred at a load of 6760 lb.

Replicate values of G_{nc} and K_{nc}, calculated from the crack pop-in stress and initial crack lengths for shear-cracked specimens of 7075-T6 aluminum sheet, 0.090 in. thick, are shown in the following tabulation:

	G_{nc} lb/in.	K_{nc} psi$\sqrt{\text{in.}}$
	138	40,600
	148	45,800
	169	49,000
	157	47,200
	166	48,600
Avg	155	46,250

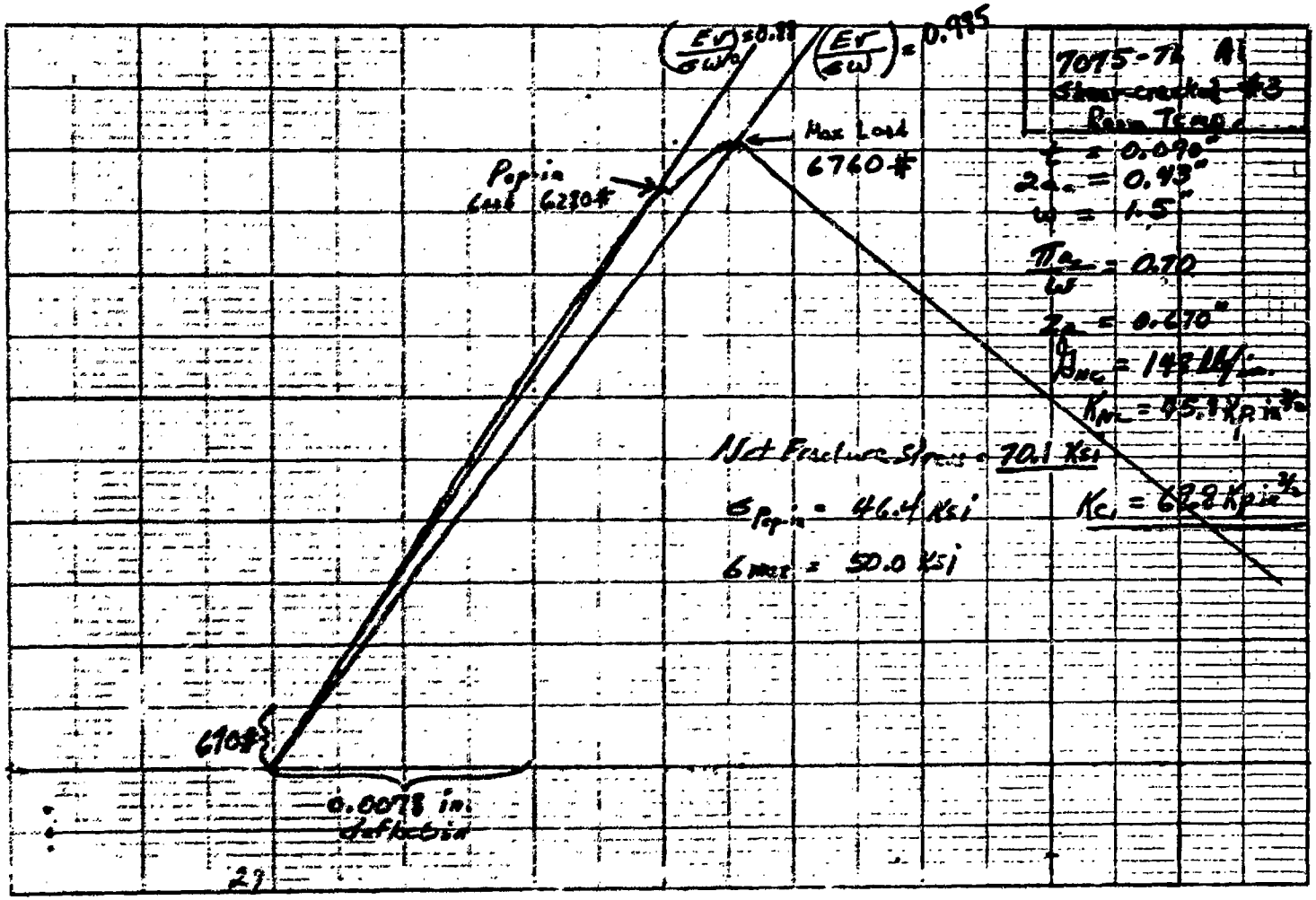

Figure 29. Compliance curve for shear-crack specimen of 7075-T6 aluminum sheet, showing crack pop-in displacement.

This average value of 155 in.-lb/in.^{2} for G_{nc} agrees fairly well with the value of about 145 in.-lb/in.^{2} for G_{Ic} reported by Krafft and Boyle (10) for large diameter (2 to 4 in.) circumferentially-notched bars of 7075-T6 aluminum.

It appears that the compliance gage, attached to the edges of sheet crack-propagation specimens of ordinary size (1.5 in. wide), can be reliably used to determine critical crack length for K_c or G_c determinations. It seems possible that the K_{nc} or G_{nc} value, calculated from the crack pop-in stress and the initial "crack" length, may correlate with the plane-strain toughness parameters, K_{Ic} and G_{Ic}, although certain requirements for the specimen have yet to be clarified.

VII. CONCLUSIONS

1. The nickel-base super alloys—Rene' 41, Nimonic 90, Inconel-X, and Unitemp 1753—all showed a slight tendency toward brittleness in the particular elevated temperature range in which these materials are usually "aged" as a part of their heat treatments. This "brittleness" tendency was manifested by a decrease in the ratio of net fracture stress to yield strength, this ratio becoming less than unity at temperatures generally from 1000° F to 1400° F, depending upon the alloy. The austenitic iron-base super alloy, A-286, and the cobalt-base alloy L 605, did not show this brittleness tendency over the temperature range of their usual service exposure—that is, up to about 1600° F.

2. Among the refractory metals, tungsten sheet, prepared from pressed-and-sintered powder, had a brittle-ductile transition temperature in the range from 300° F to 500° F. The brittle-ductile transition temperatures for sheet specimens of unalloyed molybdenum, molybdenum 1/2%-titanium, and TZM molybdenum, were respectively 150° F, 65° F, and 65° F. The two columbium-base alloys—D-14 and FS-82—were ductile over the temperature range from -300° F to 1200° F. There was some evidence of strain-aging effects in the strength properties of the refractory metals, in particular the TZM molybdenum. These effects were manifested by tensile strength maxima at certain elevated temperatures. The TZM molybdenum also exhibited a fracture-stress minimum in the strain-aging temperature range.

3. In a further investigation of similar strain-aging effects in steels, it was found that the degree of strengthening and the temperature at which the strengthening occurred were both functions of the strain rate. Increasing the strain rate increased the temperature at which the strength maximum occurred and diminished the strengthening effect. Increasing the loading rate by about five orders of magnitude either eliminated the net-fracture-stress minimum, at the strain aging temperature, or displaced this minimum to a considerably higher temperature. The occurrence of the net-fracture-stress minima in steels at strain-aging temperatures is apparently dependent upon the structural characteristics, the experimental evidence indicating that the lower strength steels are not subject to this phenomenon while the low-alloy steels heat treated to high strength levels are subject to the fracture strength minimum. In the refractory metals, no correlations between tensile-strength maxima and net-fracture-strength minima could be established.

4. Experiments with a compliance gage attached to the edges of fatigue-cracked specimens of several materials indicated that this device can be used to make reproducible determinations of critical crack length during crack-propagation tests of sheet materials at various temperatures. From these determinations direct calculations of the fracture-toughness parameters, G_c and K_c, can be made. In addition, preliminary experiments have shown that the "crack pop-in" stress, obtained by means of the compliance gage attached to shear-cracked specimens, can be used to calculate parameters, G_{nc} or K_{nc}, that appear to correlate with the plane-strain toughness parameters, G_{Ic} and K_{Ic}.

VIII. RECOMMENDATIONS

It is believed that the compliance gage should be exploited to determine the effects of various environmental conditions on the fracture toughness of important high-strength structural materials. Since the gage can be used at virtually any temperature within the usual range of service of these structural materials, the effects of temperature on the fracture-toughness parameters can be reliably determined. In addition, the effects of other variables such as loading rate, atmosphere (including very low pressures), prolonged static load, and load cycles could be evaluated in terms of fracture mechanics.

The encouraging results obtained in the "crack pop-in" experiments with shear-cracked specimens indicate that some further work would be profitable to determine whether plane-strain toughness can be reliably determined for the high-strength steels by means of these specimens.

BIBLIOGRAPHY

1. "Fracture Testing of High-Strength Sheet Materials: A Report of a Special ASTM Committee," ASTM Bulletin, January 1960, p 29.

2. Willhelm, A. Clyde, "Simultaneous Heating and Loading of Type 321 Stainless Steel and Strain Aging of Columbium and Tantalum," WADD Report 61-165, May 1961.

3. Wilcox, B. A., and Huggins, R. A., "The Effect of Interstitial Atom-Dislocation Interactions on the Deformation Behavior of Columbium, Tantalum, and 1020 Steel," Technical Documentary Report No. ASD-TR-61-351, February 1962.

4. Morrison, J. L. and Kattus, J. R., "An Investigation of Methods for Determining the Crack-Propagation Resistance of High-Strength Alloys," Summary Technical Report by Southern Research Institute to Bureau of Naval Weapons, on Contract NOas 60-6040c, March 7, 1961.

5. Cottrell, A. H., and Bilby, B. A., "Dislocation Theory of Yielding and Strain Aging of Iron," Proc. Phys. Soc., 62, 1-A, (1949), p 49.

6. Boyle, R. W., "An Instrument for Crack Growth Determinations from the Compliance of Notched Sheet Specimens," U. S. Naval Research Laboratory, Washington 25, D. C.

7. Boyle, R. W., "A Method for Determining Crack Growth in Notched Sheet Specimens," Materials Research and Standards, Vol 2, August 1962, p 646.

8. Irwin, G. R., private communication.

9. Irwin, G. R., "Fracture Testing of High-Strength Sheet Materials Under Conditions Appropriate for Stress Analysis," NRL Report 5486, July 27, 1960.

10. Boyle, R. W., "Progress in Determining K_{Ic} by the 'Pop-In' Technique," Presented at a Meeting of the ASTM Committee on Fracture Testing of High Strength Metallic Materials, NASA Lewis Research Center, August 29 and 30, 1961.

BIBLIOGRAPHY (Continued)

11. Westergaard, H. M., "Bearing Pressures and Cracks," J. Appl. Mech., Vol 6, (2) A, June 1939.

Birmingham, Alabama
November 21, 1962
5603-1256-X
(150:1:6) hmm

APPENDIX A

Data Tables
Tensile Properties and Crack-Propagation Properties

Table 4

Tensile Properties of Aged[1] Inconel-X Sheet at Different Temperatures and a Nominal Strain Rate of 5×10^{-3} in./in./min

Temp °F	0.2%-Offset Yld. Str. (ksi)	Ultimate Strength (ksi)	Elong. in 2 in. %	Final Dimensions[2] at Fracture, In. Width	Final Dimensions[2] at Fracture, In. Thickness	Reduction of Area %
75	129.0	177.5	24.0	0.304	0.051	25.7
75	134.0	163.0	23.0	0.302	0.046	43.7
Avg	131.5	170.0	23.5			30.7
300	117.0	169.2	23.0	0.304	0.054	36.4
500	107.0	156.0	23.0	0.314	0.050	36.4
500	113.0	163.5	21.5	0.303	0.052	38.7
Avg	110.0	159.5	22.3			37.5
700	101.0	153.0	22.5	0.302	0.049	40.8
900	102.5	146.5	25.0	0.301	0.055	35.7
900	116.8	160.0	25.0	0.313	0.053	35.9
Avg	109.7	153.3	25.0			35.8
1100	120.8	157.0	20.0	0.333	0.057	24.0
1100	117.0	155.0	18.5	0.329	0.058	24.4
Avg	119.0	156.0	19.3			24.2
1300	112.5	133.5	2.5	0.362	0.063	10.6
1300	113.0	134.2	2.5	0.358	0.059	14.6
Avg	112.8	133.8	2.5			12.3

Table 4 (Continued)

Tensile Properties of Aged[1] Inconel-X Sheet at Different Temperatures and a Nominal Strain Rate of 5×10^{-3} in./in./min

Temp °F	0.2%-Offset Yld. Str. (ksi)	Ultimate Strength (ksi)	Elong. in 2 in. %	Final Dimensions[2] at Fracture, In. Width	Final Dimensions[2] at Fracture, In. Thickness	Reduction of Area %
1400	107.5	120.0	2.5	0.361	0.059	12.3
1500	87.0	93.0	2.0	0.356	0.059	16.3

[1] Solution treated at 2150° F for 4 hr, air cooled; aged at 1300° F for 20 hr.
[2] Initial specimen gage dimensions were 2 in. x 0.375 in. x 0.067 in.

Table 5

Fracture Strength of Fatigue-Cracked[1], Aged[2] Inconel-X Sheet at Different Temperatures

Specimens Loaded to Failure at a Free Crosshead-Travel Rate of 0.01 in./min

Temp °F	Net Fracture Stress, ksi	Fracture Appearance Percent Shear
75	134.5	100
75	133.0	100
Avg	133.8	100
300	130.0	100
500	121.5	100
500	125.5	100
Avg	123.5	100
700	124.7	100
900	120.0	100
900	117.0	100
Avg	118.5	100
1100	110.5	100
1300	97.0	100
1300	94.0	100
Avg	95.5	100
1400	83.0	0
1400	83.0	0
Avg	83.0	0
1500	71.0	0
1500	72.0	0
1500	71.5	0

[1] Specimens 1.50 in. over-all width, 0.067 in. thick, with 0.5 in. long central fatigue crack.

[2] Solution treated at 2150° F for 4 hr, air cooled; aged at 1300° F for 20 hr.

Table 6

Tensile Properties of Aged Rene' 41 Sheet[1] at Different Temperatures and at a Nominal Strain Rate of 5×10^{-3} in./in./min

Temp °F	0.2%-Offset Yld. Str. ksi	Ultimate Strength ksi	Elong. in 2 in. %	Final Dimensions[2] at Fracture, In. Width	Final Dimensions[2] at Fracture, In. Thickness	Reduction of Area %
75	135	182	15.0	0.333	0.0719	22.4
75	144	184	15.5	0.334	0.0738	20.1
Avg	139	183	15.2			21.2
1000	125	–	–	–	–	–
1000	121	163	21.0	0.331	0.0682	25.9
Avg	123	163	21.0			25.9
1200	123		–			
1200	121	167	15.0	0.344	0.0719	20.8
1200	121	160	12.0	0.349	0.0709	19.4
Avg	122	164	13.5			20.1
1400	116	145	12.5	0.336	0.0726	20.8
1400	118	148	10.5	0.335	0.0734	19.8
Avg	117	146	11.5			20.3
1600	88.5	96.0	10.0	0.307	0.0602	39.6
1600	93.5	98.5	9.5	0.307	0.0614	38.3
Avg	91.0	97.2	9.8			39.0

[1] Solution treated at 1950° F in argon for 30 min, air quenched; aged at 1400° F for 16 hours in air, air cooled.

[2] Original specimen dimensions were 2 in. x 0.375 in. x 0.082 in.

Table 7

Fracture Strength of Fatigue-Cracked[1] Aged[2] Rene' 41 Sheet at Different Temperatures

Specimen Loaded to Failure at a Free Crosshead-Travel Rate of 0.01 in./min

Temp °F	Net Fracture Stress, ksi	Fracture Appearance Percent Shear
75	146	100
75	146	100
Avg	146	100
1000	127	100
1000	134	100
Avg	130	100
1200	131	100
1200	132	100
Avg	132	100
1400	117	100
1400	114	100
Avg	116	100
1600	92.6	100
1600	92.5	100
Avg	92.6	100

[1] Specimens 1 1/2 in. over-all width, 0.082-in. thick, with 0.5 in. long central fatigue crack.

[2] Solution treated at 1950° F in argon for 30 min air quenched, aged at 1400° F for 16 hours in air, air cooled.

Table 8

Tensile Properties of Aged[1] Unitemp 1753 Sheet at Different Temperatures and at a Nominal Strain Rate of 5×10^{-3} in./in./min

Temp °F	0.2%-Offset Yld. Str. ksi	Ultimate Strength ksi	Elong. in 2 in. %	Final Dimensions[2] at Fracture, In. Width	Final Dimensions[2] at Fracture, In. Thickness	Reduction of Area %
75	121.8	184.0	24.0	0.319	0.052	26.7
1000	109.5	153.0	24.0	0.329	0.052	18.3
1200	112.5	157.5	17.0	0.331	0.048	29.3
1400	112.5	144.0	6.5	0.366	0.055	10.7
1400	112.3	149.0	5.5			
Avg	112.4	146.5	6.0			
1600	91.0	102.0	1.5	0.364	0.052	16.0
1600	86.0	97.0	2.5	0.364	0.058	5.0
Avg	88.5	99.5	2.0			11.5
1700	76.5	81.0	3.0	0.367	0.057	7.8

[1] Solution treated at 1975° F for 4 hr, air cooled; aged at 1400° F for 2 hr.
[2] Initial specimen dimensions were 0.375 in. x 0.060 in.

Table 9

Fracture Strength of Fatigue-Cracked[1], Aged[2] Unitemp 1753 Sheet at Different Temperatures

Specimens Loaded to Failure at a Free Crosshead-Travel Rate of 0.01 in. /min

Temp ° F	Net Fracture Stress, ksi	Fracture Appearance Percent Shear
75	139.0	100
1000	127.0	100
1000	128.0	100
Avg	127.5	100
1200	127.0	100
1200	123.5	100
Avg	125.3	100
1400	115.0	95
1400	117.0	100
Avg	116.0	97.5
1450	105.5	100
1500	76.5	0
1500	78.0	0
Avg	77.3	0
1600	80.0	0

[1] Specimens 1.50 in. over-all width, 0.060 in. thick, with 0.5 in. long central fatigue crack.

[2] Solution treated at 1975° F for 4 hr, air cooled; aged at 1400° F for 2 hr.

Table 10

Tensile Properties of Aged[1] Nimonic 90 Sheet at Different Temperatures and a Nominal Strain Rate of 5×10^{-3} in./in./min

Temp °F	0.2%-Offset Yld. Str. (ksi)	Ultimate Strength (ksi)	Elong. in 2 in. %	Final Dimensions[2] at Fracture, In. Width	Final Dimensions[2] at Fracture, In. Thickness	Reduction of Area %
73	103.0	159.0	21.5	0.321	0.043	26.7
75	98.0	151.0	16.0	0.340	0.042	20.5
Avg	100.5	155.0	18.0			23.6
1000	86.0	134.0	21.5	0.327	0.037	35.5
1000	70.0	121.0	24.0	0.307	0.035	43.0
Avg	78.0	126.0	23.7			39.2
1125	90.0	133.7	16.5	0.324	0.039	31.7
1200	86.0	121.0	11.5	0.345	0.043	21.0
1200	88.5	-	6.5	0.358	0.046	12.3
Avg	87.3	121.0	9.0			16.7
1300	77.6	102.0	5.5	0.360	0.046	24.5
1400	82.0	93.0	3.0	0.357	0.045	13.0
1400	88.5	101.8	4.0	0.359	0.048	8.2
Avg	85.3	97.4	3.5			10.6
1500	80.5	88.5	2.0	0.367	0.045	12.0

[1] Solution treated at 1975° F for 8 hr, air cooled; aged at 1300° F for 16 hr.
[2] Initial specimen gage dimensions were 2 in. x 0.375 in. x 0.050 in.

Table 11

Fracture Strength of Fatigue-Cracked[1], Aged[2] Nimonic 90 Sheet at Different Temperatures

Specimens Loaded to Failure at a Free Crosshead-Travel Rate of 0.01 in./min

Temp °F	Net Fracture Stress, ksi	Fracture Appearance Percent Shear
75	137.5	100
75	129.5	100
Avg	133.5	100
1000	118.0	100
1000	118.0	100
Avg	118.0	100
1200	104.0	100
1200	98.0	100
Avg	101.0	100
1250	86.0	0
1300	79.5	20.0
1400	79.5	0
1400	76.5	0
Avg	78.0	0
1450	69.5	0
1500	59.0	0

[1] Specimens 1 1/2 in. over-all width, 0.050 in. thick, with 0.50 in. long central fatigue cracks.

[2] Solution treated at 1975° F for 8 hr, air cooled; aged at 1300° F for 16 hr.

Table 12

Tensile Properties of Aged[1] A-286 Alloy Sheet[2] at Different Temperatures and at a Nominal Strain Rate of 0.005 in./in./min

Temp °F	0.2%-Offset Yld. Str. (ksi)	Ultimate Str. (ksi)	Elong. 2 in. %
75	66.0	142.0	27.5
75	74.0	148.0	26.0
75	67.0	137.6	27.0
Avg	69.0	142.5	26.8
500	68.8	137.6	22.5
500	68.8	132.4	20.0
Avg	68.8	135.0	21.25
1000	68.8	116.9	0
1000	67.0	116.9	20.0
Avg	67.9	116.9	20.0
1500	15.5	27.5	30.0
1500	17.2	22.3	25.0
Avg	16.35	24.9	25.0

[1] Solution treated at 1800° F for 1 hr, oil quenched; aged at 1325° F for 16 hr.

[2] Tensile specimens with gage sections 2 in. long, 3/8 in. wide, and 0.040 in. thick.

Table 13

Fracture Strength of Fatigue-Cracked Aged[1] A 286 Alloy Sheet[2] at Different Temperatures

Specimens Loaded to Failure at a Free Crosshead-Travel Rate of 0.01 in./min

Temp °F	Net Fracture Stress, ksi	Fracture Appearance, Percent Shear
75	99.5	100
75	109.0	100
75	108.5	100
Avg	105.6	
500	99.3	100
500	95.0	100
Avg	97.1	
1000	93.0	100
1000	89.6	100
Avg	91.3	
1500	46.0	100
1500	45.7	100
Avg	45.9	

[1] Solution treated at 1800° F for 1 hr, oil-quenched; aged at 1325° F for 16 hr.

[2] Sheet thickness 0.040 in.; specimens 1.5 in. wide, with central fatigue cracks 0.52 in. to 0.55 in. in over-all length.

Table 14

Tensile Properties of Annealed L 605 Cobalt-Base Alloy Sheet[1] at Different Temperatures[2]

Temp °F	0.2%-Offset Yld. Str. KSI	Ultimate Str. KSI	Elong. in 2 in. %
75	69.5	140.5	51.0
75	68.0	140.0	66.0
75	76.0	138.0	54.0
Avg	71.2	139.5	57.0
500	44.6	117.0	75.0
500	45.75	116.0	67.0
500	42.6	115.0	71.0
Avg	44.3	116.0	68.0
1000	33.5	98.9	64.0
1000	34.8	100.0	63.0
1000	36.5	102.0	61.0
Avg	34.9	100.3	62.6
1600	26.4	45.5	12.5
1600	30.0	46.0	12.0
1600	27.5	35.5	12.5
Avg	27.9	43.0	12.3

[1] Tensile specimens with gage section 2 in. long, 3/8 in. wide, and 0.045 in. thick.

[2] Specimens held at elevated temperature for 1 min before loading to failure.

Table 15

Fracture Strength of Fatigue-Cracked Annealed L 605 Cobalt-Base Alloy Sheet[1] at Different Temperatures[2]

Temp °F	Net Fracture Stress, ksi
75	93.0
75	93.0
Avg	93.0
500	62.0
500	66.7
Avg	64.3
1000	59.5
1000	62.0
1000	60.0
Avg	60.5
1600	41.5
1600	40.0
1600	41.0
Avg	40.8

[1] Sheet thickness 0.045 in.; specimens 1.5 in. wide, with central fatigue cracks 0.51 in. to 0.58 in. in over-all length.

[2] Specimens held at elevated temperature for 1 min before loading to failure.

Table 16

Tensile Strength Properties of Unalloyed Tungsten Sheet[1] at Various Temperatures

Temp °F	0.2%-Offset Yld. Str. (ksi)	Ultimate Strength (ksi)	Elong. in 2 in. %	Final Dimensions[2] at Fracture, In. Width	Final Dimensions[2] at Fracture, In. Thickness	Reduction of Area %
75	–[3]	154	–	–	–	–
1000	93.0	109	2.5	0.362	0.030	33
1500	83.0	92.5	3.0	0.369	0.027	37
1550	–	102	2.5	0.368	0.030	29
1600	86.0	95.0	2.5	0.368	0.029	32
1600	91.9	93.0	2.5	0.367	0.025	40
Avg	89.0	94.0	2.5	–	–	36
1750	83.0	92.5	2.0	0.364	0.020	54
1850	86.5	90.0	1.5	0.362	0.024	42
2000	73.8	83.8	2.0	–	–	–[4]
2200	65.5	78.5	2.5	0.371	0.023	45

[1] Tungsten sheet prepared by the powder metallurgy method; hot-rolled and stress-relieved at 1830° F for 25 min.
[2] Initial dimensions of specimen gage section were 2 in. x 0.375 x 0.041 in.
[3] Specimen did not yield.
[4] Fracture had knife-edge appearance.

Table 17

Fracture Strength Properties of Sharply Notched Unalloyed Tungsten Sheet[1]

Temp °F	Net Fracture Stress ksi
300	> 91[2]
400	> 102[2]
600	108
800	102
1000	96.3
1200	91.5

[1] Specimens 1.5 in. in over-all width and 0.041 thick with 0.5 in. central notches. The radii of the notch roots were nominally 0.0005 in.

[2] Specimen fractured in the grips rather than at the notch. Value shown represents stress level in the notched section at the time fracture occurred in the pin-hole and may be regarded as a lower limit of net fracture stress.

Table 18

Tensile Properties of Unalloyed Molybdenum Sheet[1] at Different Temperatures and at a Nominal Strain Rate of 5×10^{-3} in./in./min

Temp °F	0.2%-Offset Yld. Str. ksi	Ultimate Strength ksi	Elong. in 2 in. %	Final Dimensions[2] at Fracture, in. Width	Final Dimensions[2] at Fracture, in. Thickness	Reduction of Area %
80	97.0	99.5	46.5	0.300	0.034	54.0
600	53.7	69.0	10.0	0.310	0.031	55.9
800	62.1	64.5	6.0	0.327	0.037	44.5
1100	55.0	62.1	6.0	0.314	0.028	59.6
1300	55.0	59.8	5.0	0.324	0.027	61.5
1500	55.3	55.3	6.0	0.318	0.032	53.2

[1] Stress-relieved
[2] Initial specimen gage dimensions were: 2 in. x 0.375 in. x 0.060 in.

Table 19

Fracture Strength of Fatigue-Cracked Unalloyed Molybdenum Sheet[1] at Different Temperatures and at a Crosshead-Travel Rate of 0.01 in./min

Temp °F	Net Fracture Stress, ksi	Fracture Toughness, K_c', ksi $\sqrt{in.}$
0	27.3	15.6
75	48.8	28.0
75	97.5	58.2
75	53.0	28.5
Avg	66.4	38.2
150	85.0	47.8
150	82.0	47.8
Avg	83.5	47.8
200	77.0	-
200	74.0	-
Avg	75.5	
300	82.0	-

[1] Stress-relieved

Table 20

Tensile Properties of Molybdenum 1/2%-Titanium Alloy Sheet[1] at Different Temperatures and at a Nominal Strain Rate of 5×10^{-3} in./in./min

Temp °F	0.2%-Offset Yld. Str. (ksi)	Ultimate Strength (ksi)	Elong. in 2 in. %	Final Dimensions[2] at Fracture, in. Width	Final Dimensions[2] at Fracture, in. Thickness	Reduction of Area %
80	128.0	134.0	11.5	0.330	0.040	44.7
500	92.0	102.5	7.5	0.342	0.036	34.3
600	89.0	99.5	5.0	0.344	0.044	37.0
700	88.0	96.5	4.5	0.345	0.038	45.2
800	91.0	100.5	4.0	0.341	0.047	33.0
900	88.0	98.5	3.0	0.344	0.045	35.1
900	83.5	92.0	4.0	0.343	0.039	44.0
Avg	85.8	95.3	3.5	0.344	0.042	38.5

[1] Stress-relieved.
[2] Initial specimen gage dimensions were 2 in. x 0.375 in. x 0.064 in.

Table 21

Fracture Strength of Fatigue-Cracked Molybdenum 0.5%-Titanium Alloy Sheet[1] at Different Temperatures and at a Crosshead-Travel Rate of 0.01 in./min

Temp °F	Net Fracture Stress, ksi	Fracture Toughness, Kc', ksi $\sqrt{\text{in.}}$
6	39.2	23.1
25	113.0	68.1
45	129.0	80.1
45	84.0	51.6
Avg	107.0	65.8
80	114.5	69.5
700	93.5	-
700	94.0	-
Avg	93.8	
800	100.0	-
800	100.0	-
Avg	100.0	
900	85.0	-

[1] Stress-relieved

Table 22

Tensile Properties of Molybdenum 0.5%-Titanium 0.08%-Zirconium Alloy Sheet[1] at Different Temperatures and at a Nominal Strain Rate of 5×10^{-3} in./in./min

Temp °F	0.2%-Offset Yld. Str. (ksi)	Ultimate Strength (ksi)	Elong. in 2 in. %	Final Dimensions[2] at Fracture, In. Width	Final Dimensions[2] at Fracture, In. Thickness	Reduction of Area %
77	147.0	150.0	7.0	0.354	0.055	15.8
500	108.0	119.5	2.5	0.358	0.050	22.7
600	109.0	117.8	2.0	0.360	0.048	24.0
715	103.2	112.0	2.0	0.359	0.044	32.2
800	108.0	115.2	1.5	0.359	0.050	22.5
900	106.5	112.0	1.5	0.363	0.042	25.8
1000	108.5	137.0	2.0	0.361	0.051	17.8
1100	102.0	128.0	1.5	0.335	0.046	33.5

[1] Stress-relieved.
[2] Initial specimen gage dimensions were 2 in. x 0.375 in. x 0.060 in.

Figure 23

Fracture Strength of Fatigue-Cracked Molybdenum 0.5%-Titanium 0.08%- Zirconium Alloy Sheet[1] at Different Temperatures and at a Crosshead-Travel Rate of 0.01 in./min

Temp °F	Net Fracture Stress, ksi	Fracture Toughness K_c, ksi $\sqrt{\text{in.}}$
-50	47.5	28.4
-50	48.0	29.5
Avg	47.8	29.0
10	51.0	36.6
20	95.0	61.6
78	136.0	78.7
78	129.5	77.5
Avg	132.8	78.1
500	120.0	-
800	110.5	-
900	101.4	-
1000	98.0	-
1100	103.0	-

[1] Stress-relieved.

Table 24

Standard Tensile Properties of D-14[1] Columbium Alloy Sheet at Various Temperatures

Temp °F	0.2%-Offset Yld. Str. ksi	Ultimate Strength ksi	Elong. in 2 in. %	Final Dimensions[2] at Fracture, In. Width	Final Dimensions[2] at Fracture, In. Thickness	Reduction of Area %
-300	100	107	7	0.142[3]	0.020	65
-200	80	80.4	11	0.170[4]	0.020	67
-100	68.8	80.8	9	0.172[5]	0.028	54
75	56.2	66.8	18	0.213	0.023	62
75	52.0	67.6	18	0.217	0.019	67
Avg	54.1	67.2	18	-	-	64
200	48.1	61.4	17	0.218	0.023	60
200	45.0	61.6	17	0.221	0.022	62
Avg	46.6	61.5	17	-	-	61
300	41.7	56.8	16	0.219	0.022	62
400	45.9	55.7	14	0.225	0.015	74
400	38.8	54.1	13	0.214	0.026	56
Avg	42.4	54.9	14	-	-	65
450	38.6	54.8	12	0.216	0.016	71
450	41.7	53.0	14	0.216	0.020	67
Avg	40.2	53.9	13	-	-	69
500	38.5	52.7	12	0.226	0.025	57
500	43.7	52.0	13	0.218	0.021	64
Avg	41.1	52.4	12	-	-	60

Table 24 (Continued)

Standard Tensile Properties of D-14[1] Columbium Alloy Sheet at Various Temperatures

Temp °F	0.2%-Offset Yld. Str. ksi	Ultimate Strength ksi	Elong. in 2 in. %	Final Dimensions[2] at Fracture, In. Width	Final Dimensions[2] at Fracture, In. Thickness	Reduction of Area %
550	41.1	52.2	12	0.234	0.015	72
550	44.6	52.5	10	0.218	0.025	55
Avg	42.8	52.4	11	-	-	64
600	40.8	53.9	11	0.218	0.026	54
600	38.2	53.4	12	0.220	0.014	75
600	40.5	52.5	11	0.220	0.018	68
600	37.4	53.7	12	0.222	0.014	75
Avg	39.2	53.4	12	-	-	68
650	36.9	52.4	11	0.233	0.026	52
650	43.7	52.9	11	0.229	0.019	65
650	40.8	51.6	11	0.224	0.026	55
Avg	40.1	52.3	11	-	-	57
700	40.5	52.9	10	0.224	0.033	38
700	37.0	51.1	11	0.231	0.020	65
Avg	38.8	52.0	10	-	-	52
750	38.8	52.2	8	0.222	0.017	68
750	37.8	52.2	9	0.256	0.025	54
Avg	38.3	62.2	8	-	-	61
800	40.3	51.8	11	0.224	0.029	49
800	34.1	52.1	12	0.237	0.018	67
Avg	37.2	52.0	12	-	-	58

Table 24 (Continued)

Standard Tensile Properties of D-14[1] Columbium Alloy Sheet at Various Temperatures

Temp °F	0.2%-Offset Yld. Str. ksi	Ultimate Strength ksi	Elong. in 2 in. %	Final Dimensions[2] at Fracture, In. Width	Final Dimensions[2] at Fracture, In. Thickness	Reduction of Area %
900	40.5	52.1	9	0.221	0.026	52
900	36.9	52.8	9	0.218	0.020	65
Avg	38.7	52.4	9	–	–	58
1000	40.6	53.8	9	0.242	0.030	42
1000	40.9	51.7	9	0.236	0.017	69
Avg	40.8	52.8	9	–	–	56
1050	42.1	53.8	8	0.242	0.028	45
1050	37.9	53.4	8	0.240	0.015	71
Avg	40.0	53.6	8	–	–	58
1100	45.8	53.0	7	0.235	0.022	58
1100	44.2	53.1	7	0.235	0.027	48
Avg	45.0	53.0	7	–	–	53
1150	38.6	52.5	7	0.238	0.026	51
1150	37.4	52.4	8	0.230	0.029	47
Avg	38.0	52.4	8	–	–	49
1200	37.1	50.8	7	0.238	0.031	43
1200	43.1	52.4	7	0.237	0.033	38
Avg	40.1	51.6	7	–	–	40

[1] Cold-rolled and stress-relieved.
[2] Nominal original specimen gage section dimensions 2 in. × 0.62 in. × 0.050 in.
[3] Specimen original width reduced to 0.166 in.
[4] Specimen original width 0.202 in.
[5] Specimen original width 0 [illegible] in.

Table 25

Fracture Strength of Fatigue-Cracked[1] D-14 Sheet[2] at Various Temperatures

Temp °F	Net Fracture Stress ksi
-300	95.7
-200	83.5
-100	76.3
75	62.7
200	58.4
400	52.6
600	49.5
600	48.1
Avg	48.8
700	49.1
700	49.7
Avg	49.4
800	49.7
800	48.8
Avg	49.2
900	50.4
900	49.9
Avg	50.2
1000	49.3
1000	52.4
1000	51.6
1000	48.1
Avg	50.4

Table 25 (Continued)

Fracture Strength of Fatigue-Cracked[1] D-14 Sheet[2] at Various Temperatures

Temp °F	Net Fracture Stress ksi
1100	52.1
1100	52.5
1100	51.1
Avg	51.9
1200	47.6
1200	50.3
Avg	49.0

[1] Sheet specimens 0.050 in. thick, 1.500 in. in overall width, with central transverse fatigue cracks nominally 0.500 in. in length.
[2] Cold-rolled and stress-relieved.

Table 26

Standard Tensile Properties of FS 82 Sheet[1] at Various Temperatures

Temp °F	0.2%-Offset Yld. Str. ksi	Ultimate Strength ksi	Elong. in 2 in. %	Final Dimensions[2] at Fracture, In. Width	Final Dimensions[2] at Fracture, In. Thickness	Reduction of Area %
-200	60.2	>83.7	–[3]	–	–	–
-200	56.4	>79.8	–[3]	–	–	–
Avg	58.3	>81.8	–[3]	–	–	–
75	38.2	61.8	21	0.215	0.026	42
200	37.2	56.0	19	0.210	0.020	58
400	31.8	49.5	17	0.218	0.014	68
600	33.2	49.1	15	0.205	0.018	62
800	30.8	48.6	10	0.218	0.021	54
800	29.5	46.1	11	0.207	0.015	68
Avg	30.2	47.4	10	–	–	
900	25.5	46.7	11	0.226	0.015	66
900	32.7	43.7	8	0.234	0.015	64
Avg	29.1	45.2	10	–	–	65
1000	28.3	47.7	10	0.227	0.022	50
1000	31.2	50.2	10	0.222	0.014	69
Avg	29.8	49.0	10	–	–	60
1100	31.3	50.3	7	0.237	0.018	56
1100	33.5	50.1	7	0.241	0.019	54
Avg	32.4	50.2	7	–	–	55

Table 26 (Continued)

Standard Tensile Properties of FS 82 Sheet[1] at Various Temperatures

Temp °F	0.2%-Offset Yld. Str. (ksi)	Ultimate Strength (ksi)	Elong. in 2 in. %	Final Dimensions[2] at Fracture, In. Width	Final Dimensions[2] at Fracture, In. Thickness	Reduction of Area %
1200	26.8	48.5	7	0.242	0.025	39
1200	29.9	51.5	5	0.247	0.029	29
Avg	28.4	50.0	6	–	–	34
1250	31.1	50.7	6	0.241	0.031	25
1300	29.4	44.7	4	0.243	0.032	22
1300	25.0	46.0	7	0.234	0.038	8
Avg	27.2	45.4	6	–	–	15
1400	28.7	49.0	5	0.242	0.035	16

[1] Hot-rolled and stress-relieved.
[2] Initial dimensions of specimen gage section were nominally 2 in. x 0.25 in. x 0.040 in.
[3] Specimen fractured outside of gage section. The ultimate strength shown for this specimen represents the stress present in the gage section at failure and should therefore be regarded as a lower limit of the ultimate strength.

Table 27

Fracture Strength of Fatigue-Cracked[1] FS 82 Sheet[2] at Various Temperatures

Temp °F	Net Fracture Stress ksi
-320	>83.7[3]
-200	71.3
-100	59.8
75	50.3
300	47.0
450	39.3
525	39.7
600	38.4
700	40.2
800	39.5
900	38.9
1000	41.3
1050	41.3
1175	38.5
1300	38.7

[1] Specimens 1 1/2 in. in over-all width, 0.040 in. thick, with 0.5 in. central fatigue crack.

[2] Hot-rolled and stress-relieved.

[3] Specimen fractured in the grip where the temperature was higher. The value given represents stress on the fatigue-cracked section at the time fracture occurred in the pin-hole and should be regarded as a lower limit for the fracture stress.

Table 28

Tensile Properties of Tempered[1] AISI 4130 Steel at Different Temperatures and at a Strain Rate of 1×10^{-5} in./in./sec

Temp °F	0.2%-Offset Yld. Str. (ksi)	Ultimate Strength (ksi)	Elong. in 2 in. %	Final Dimensions[2] at Fracture, In. Width	Thickness	Reduction of Area %
-100	218	256	5.0	0.355	0.031	28
-100	223	256	5.5	0.357	0.031	31
Avg	220	256	5.2			29
75	216	255	5.0	0.361	0.030	30
75	216	255	4.5	0.358	0.026	40
Avg	216	255	4.8			35
170	215	260	5.0	0.358	0.032	25
170	200	250	5.0	0.362	0.036	15
Avg	208	255	5.0			20
200	200	260	5.0	0.365	0.037	12
200	215	275	4.5	0.364	0.034	17
Avg	208	268	4.8			14
250	186	263	5.0	0.368	0.035	19
300	181	260	7.0	0.344	0.036	19
350	176	252	7.5	0.345	0.037	20
400	181	241	7.5	0.324	0.032	31

[1] Austenitized at 1570° F in argon for 30 min, oil quenched; tempered at 400° F in air for 2 hours, air cooled.

[2] Nominal original specimen dimension were 2 in. x 0.375 in. x 0.040 in.

Table 29

Tensile Properties of Tempered[1] AISI 4130 Steel at Different Temperatures and a Strain Rate of 5×10^{-3} in./in./sec

Temp °F	0.2%-Offset Yld. Str. ksi	Ultimate Strength ksi	Elong. in 2 in. %	Final Dimensions[2] at Fracture, In. Width	Thickness	Reduction of Area %
-100	226	284	6.0	0.356	0.035	20
-100	238	262	5.0	0.355	0.032	28
Avg	232	273	5.5			24
-50	224	257	5.5	0.358	0.032	28
-50	235	261	4.5	0.362	0.027	38
Avg	230	259	5.0			33
75	220	250	4.0	0.353	0.033	25
200	216	245	4.0	0.361	0.036	16
300	–	245	4.0	0.358	0.039	9
300	200	245	5.0	0.363	0.034	22
Avg	200	245	4.5			16
350	200	248	4.0	0.366	0.037	16
350	196	250	5.0	0.352	0.036	18
Avg	198	249	4.5			17
400	186	255	4.0	0.369	0.034	19
400	196	260	5.5	0.350	0.09	11
Avg	191	258	4.8			15
450	181	252	6.5	0.341	0.036	23
450	191	252	6.5	0.337	0.034	19
Avg	186	252	6.5			21

Table 29 (Continued)

Tensile Properties of Tempered[1] AISI 4130 Steel at Different Temperatures and at a Strain Rate of 5×10^{-3} in./in./sec

Temp °F	0.2%-Offset Yld. Str. ksi	Ultimate Strength ksi	Elong. in 2 in. %	Final Dimensions[2] at Fracture, In. Width	Final Dimensions[2] at Fracture, In. Thickness	Reduction of Area %
600	157	210	8.0	0.326	0.030	38

[1] Austenitized at 1570° F in argon for 30 min, oil quenched; tempered at 400° F in air for 2 hours, air cooled.

[2] Nominal original specimen dimension was 2 in. x 0.375 in. x 0.040 in.

Table 30

Tensile Properties of Tempered[1] AISI 4130 Steel at Different Temperatures and at a Strain Rate of 0.5 in./in./sec

Temp °F	0.2%-Offset Yld. Str. ksi	Ultimate Strength ksi	Elong. in 2 in. %	Final Dimensions[2] at Fracture, In. Width	Thickness	Reduction of Area %
-100	-	289	6.0	0.357	0.035	19
-100	234	268	5.0	0.360	0.031	28
-100	255	285	5.0	0.361	0.030	30
Avg	244	281	5.3			26
-50	-	274	5.0	0.359	0.035	19
-50	234	263	4.0	0.364	0.035	18
-50	-	270	5.0	0.363	0.037	13
Avg	234	269	4.7			17
75	221	259	5.0	0.364	0.034	22
75	221	260	5.0	0.361	0.025	42
Avg	221	260	5.0			32
200	210	248	5.0	0.359	0.034	23
300	212	241	3.5	0.363	0.034	22
300	206	249	4.0	0.362	0.034	22
Avg	209	245	3.8			22
325	204	247	4.0	0.364	0.035	20
350	197	236	3.5	0.363	0.031	29
350	201	242	4.0	0.360	0.033	23
Avg	199	239	3.8			26
375	192	238	4.0	0.363	0.037	15

Table 30 (Continued)

Tensile Properties of Tempered[1] AISI 4130 Steel at Different Temperatures and at a Strain Rate of 0.5 in./in./sec

Temp °F	0.2%-Offset Yld. Str. ksi	Ultimate Strength ksi	Elong. in 2 in. %	Final Dimensions[2] at Fracture, In. Width	Final Dimensions[2] at Fracture, In. Thickness	Reduction of Area %
400	191	225	3.0	0.363	0.035	19

[1] Austenitized at 1570° F in argon for 30 min, oil quenched; tempered at 400° F in air for 2 hours, air cooled.

[2] Nominal original specimen dimensions were 2 in. x 0.375 in. x 0.040 in.

Table 31

Fracture Strength of Fatigue-Cracked[1] Tempered[2] AISI 4130 Steel at Different Temperatures and a Loading Rate of 4 lbs/sec[3]

Temp ° F	Net Fracture Stress, ksi	Fracture Appearance Percent Shear
-240	90.3	25
-240	117	65
Avg	103	45
-200	184	100
-150	201	100
-100	194	100
75	183	100
75	185	100
Avg	184	100
170	160	100
200	158	100
250	131	100
300	112	100
350	134	100

[1] Specimens 1 1/2 in. in over-all width. 0.050 in. thick, with 0.5 in. long central fatigue crack.

[2] Austenitized at 1570° F in argon for 30 min, oil quenched; tempered at 400° F in air for 2 hours, air cooled.

[3] These specimens were fractured using the same rate of cross-travel that produced a strain rate of 1×10^{-5} in./in./sec in the standard tensile specimens.

Table 31

Fracture Strength of Fatigue-Cracked[1] Tempered[2] AISI 4130 Steel at Different Temperatures and a Loading Rate of 4 lbs/sec[3]

Temp ° F	Net Fracture Stress, ksi	Fracture Appearance Percent Shear
-240	90.3	25
-240	117	65
Avg	103	45
-200	184	100
-150	201	100
-100	194	100
75	183	100
75	185	100
Avg	184	100
170	160	100
200	158	100
250	131	100
300	112	100
350	134	100

[1] Specimens 1 1/2 in. in over-all width. 0.050 in. thick, with 0.5 in. long central fatigue crack.

[2] Austenitized at 1570° F in argon for 30 min, oil quenched; tempered at 400° F in air for 2 hours, air cooled.

[3] These specimens were fractured using the same rate of cross-travel that produced a strain rate of 1 x 10^{-5} in./in./sec in the standard tensile specimens.

Table 32

Fracture Strength of Fatigue-Cracked[1] Tempered[2] AISI 4130 Steel at Different Temperatures and a Loading Rate of 2×10^3 lb/sec[3]

Temp ° F	Net Fracture Stress, ksi	Fracture Appearance Percent Shear
-240	93.9	80
-240	96.0	30
Avg	95.0	55
-200	160	100
-200	181	100
Avg	172	100
-150	200	100
-100	200	100
75	196	100
200	179	100
250	134	100
300	131	100
350	155	100
400	140	100

[1] Specimen 1 1/2 in. in over-all width, 0.050 in. thick, with 0.5 in. long central fatigue crack.

[2] Austenitized at 1570° F in argon for 30 min, oil quenched; tempered at 400° F in air for 2 hours, air cooled.

[3] These specimens were fractured using the same rate of crosshead travel that produced a strain rate of 5×10^{-3} in./in./sec in the standard tensile specimens.

Table 33

Fracture Strength of Fatigue-Cracked[1] Tempered[2] AISI 4130 Steel at Different Temperatures and a Loading Rate of 2×10^5 lbs/sec[3]

Temp ° F	Net Fracture Stress, ksi	Fracture Appearance Percent Shear
-240	86.5	35
-240	98.0	50
Avg	92.2	42
-200	163	100
-150	209	100
-125	205	100
-100	220	100
75	206	100
200	198	100
300	183	100
400	162	100
400	180	100
Avg	171	100
450	131	100
500	135	100
500	78	100
Avg	106	100

1 Specimens 1 1/2 in. in over-all width 0.050 in. thick, with 0.5 in. long central fatigue crack.

2 Austenitized at 1570° F in argon for 30 min, oil quenched; tempered at 400° F in air for 2 hours, air cooled.

3 These specimens were fractured using the same rate of crosshead travel that produced a strain rate of 0.5 in./in./sec in the standard tensile specimens.

Table 34

Tensile Properties of Hot-Rolled AISI 1020 Steel Sheet at Various Temperatures at a Nominal Strain Rate of 0.2 in./in./sec

Temp °F	0.2%-Offset Yld. Str. ksi	Ultimate Strength ksi	Elong. in 2 in. %	Final Dimensions[2] at Fracture, In. Width	Final Dimensions[2] at Fracture, In. Thickness	Reduction of Area %
-320	-[3]	147.0	-[2]	0.373	0.065	0
-200	103.0	110.0	17.5	0.346	0.042	42
80	51.3	-[3]	24.0	0.300	0.043	47
80	56.6	83.5	25.0	0.286	0.040	53
Avg	53.9	83.5	24.5			50
200	47.6	76.6	20.0	0.287	0.042	52
300	43.1	71.6	23.5	0.281	0.043	51
350	40.9	71.4	21.5	0.294	0.045	46
400	40.9	66.2	22.0	0.285	0.039	55
450	41.7	67.4	21.5	0.290	0.044	47

[1] Nominal original specimen gage-section dimensions were 2 in. x 0.375 in. x 0.065 in.
[2] Specimen fractured without yielding.
[3] Load record incomplete.

Table 35

Fracture Strength of Fatigue-Cracked[1], Hot-Rolled AISI 1020 Steel Sheet at Different Temperatures and a Nominal Loading Rate of 2×10^{-6} lb/sec[2]

Temp °F	Net Fracture Stress, ksi	Fracture Appearance Percent Shear
-320	48	0
-250	44	0
-100	89	100
80	75	100
200	75	100
300	73	100
400	69	100

1 Specimens 1 1/2 in. in over-all width, 0.065 in. thick, with 0.50 in. long central fatigue crack.

2 These specimens were fractured using the same rate of crosshead travel that produced a strain rate of 0.2 in./in./sec in the standard tensile specimens.

Table 36

Tensile Properties of Hot-Rolled AISI 1020 Steel Sheet at Various Temperatures at a Nominal Strain Rate of 1×10^{-5} in./in./sec

Temp °F	0.2%-Offset Yld. Str. (ksi)	Ultimate Strength (ksi)	Elong. in 2 in. %	Final Dimensions[2] at Fracture, In. Width	Final Dimensions[2] at Fracture, In. Thickness	Reduction of Area %
-320	122.0	127.0	16.5	0.338	0.060	17
80	44.3	68.2	24.0	0.302	0.044	45
200	45.8	71.7	23.0	0.287	0.045	47
300	40.2	69.0	20.5	0.289	0.041	52
350	39.4	69.8	13.0	0.295	0.046	45
400	42.7	82.5	17.0	0.301	0.045	45
450	36.6	73.3	14.5	0.313	0.043	45

[1] Nominal original specimen gage-section dimensions were 2 in. x 0.375 in. x 0.065 in.

Table 37

Fracture Strength of Fatigue-Cracked[1], Hot-Rolled AISI 1020 Steel Sheet at Different Temperatures and a Nominal Loading Rate of 4 lb/sec[2]

Temp °F	Net Fracture Stress, ksi	Fracture Appearance Percent Shear
-320	58	0
-150	69	100
-100	63	100
80	63	100
200	55	100
300	59	100
350	59.5	100
400	60	100
450	60	100

[1] Specimens 1 1/2 in. in over-all width, 0.065 in. thick, with 0.50 in. long central fatigue crack.

[2] These specimens were fractured using the same rate of crosshead travel that produced a strain rate of 1×10^{-3} in./in./sec in the standard tensile specimens.

Table 38

Standard Tensile Properties[1] of 300 M Low-Alloy Steel[2] at Various Temperatures

Temp °F	0.2%-Offset Yld. Str. ksi	Ultimate Strength ksi	Elong. in 2 in. %	Mod. of Elast. 10^6 psi
75	257	277	4.0	28.5
75	240	273	6.0	26.6
75	242	292	5.0	29.1
75	220	274	6.0	27.1
Avg	240	279	5.3	27.8
200	211	268	5.0	26.6
200	217	273	6.0	26.3
Avg	214	270	5.5	26.5
300	203	274	4.0	26.4
300	215	279	4.0	24.5
Avg	209	276	4.0	25.5
400	204	281	6.0	24.2
400	203	283	6.0	25.1
400	204	280	7.0	24.5
Avg	204	281	6.3	24.6
500	179	265	6.0	25.6
500	187	265	4.0	23.5
Avg	184	265	5.0	24.5
600	159	228	7.0	23.5
800	136	195	6.0	22.7

[1] Nominal specimen gage-section dimensions 2 in. x 0.25 in. x 0.080 in.

[2] Austenitized at 1600° F for 30 min; oil quenched; tempered twice at 600° F for 2 hr.

Table 39

Crack-Propagation Properties[1] of 300 M Low-Alloy Steel[2] at Various Temperatures

Temp °F	Net Fracture Stress ksi	K_c ksi $\sqrt{in.}$	Percent Shear in Fracture	Critical Crack Length, in.
75	133	159	100	0.84
75	131	121	95	0.84
Avg	132	140	–	0.84
200	118	113	95	0.71
200	125	128	80	0.71
Avg	122	122	–	0.71
400	86.2	109	90	1.03
400	100	116	100	0.90
400	96.3	125	90	0.95
400	92.6	102	80	0.89
400	95.2	97.2	100	1.00
400	106	132	100	0.94
400	102	88.4	80	0.83
Avg	96.9	110	–	0.93
600	116	105	100	0.61
600	104	105	95	0.72
Avg	110	105	–	0.67
800	116	150	100	0.81

[1] Specimens 1.5 in. in over-all width, 0.080 in. thick, with central fatigue cracks nominally 0.5 in. in length.

[2] Austenitized at 1600° F for 30 min, oil quenched; tempered twice at 600° F for 2 hr.

Table 40

Standard Tensile Properties[1] of AISI 4340 Steel[2] at 350° F

	0.2%-Offset Yld. Str.	Ultimate Strength	Elong. in 2 in.	Mod. of Elast.
	ksi		%	10^6 psi
	183	280	2.1	25.2
	198	281	2.1	23.0
	189	280	2.1	23.4
Avg	190	280	2.1	23.8

[1] Nominal specimen gage-section dimensions 2 in. x 0.25 in x 0.064 in.

[2] Austenitized at 1600° F for 30 min, oil quenched; tempered twice at 400° F for 2 hr.

Table 41

Crack-Propagation Properties[1] of AISI 4340 Steel[2] at 350° F

	Net Fracture Stress ksi	K_c ksi $\sqrt{\text{in.}}$	Percent Shear in Fracture
	132	219	100
	137	273	100
	133	228	100
	120	225	100
	123	274	100
Avg	129	250	100

[1] Specimens 1.5 in. in over-all width, 0.064 in. thick, with central fatigue cracks nominally 0.5 in. in length.

[2] Austenitized at 1600° F for 30 min, oil quenched; tempered twice at 400° F for 2 hr.

APPENDIX B

Modification of the Irwin-Westergaard Compliance Equation to Reflect Compliance at the Edges of a Centrally-Cracked Specimen

Westergaard (1) has provided a convenient two dimensional stress analysis in rectangular coordinates of a very large flat plate with tension applied in the y direction and a system of cracks along the x axis each of length 2a and center at x = 0, $\pm L$, $\pm 2L$, ...

The pertinent values are given in terms of an analytic function,

$$Z = \frac{\sigma}{\sqrt{1 - \left(\frac{\sin\left(\frac{\pi a}{L}\right)}{\sin\left(\frac{\pi z}{L}\right)}\right)^2}} \quad (B1)$$

of the complex variable $z = x + iy$.

In Westergaard's notation:

$$Z = \frac{d\bar{Z}}{dz},$$

$$Z' = \frac{dZ}{dz},$$

and

$$Z = Z(z) = \text{Re } Z + i \text{ Im } Z.$$

According to this method the stresses are assumed to be functions of x and y only and are expressed as

$$\sigma_y = \text{Re } Z + y \text{ Im } Z'$$

$$\sigma_x = \text{Re } Z - y \text{ Im } Z'$$

$$\tau_{xy} = -y \text{ Re } Z';$$

and the displacement, v, in the y direction for a plane strain situation

$$Ev = 2(1 - \nu^2) \text{ Im } \bar{Z} - (1 + \nu) y \text{ Re } Z, \quad (B2)$$

where ν is Poisson's ratio and E is the modulus of elasticity.

Irwin has shown (9) that the above stress analysis is a good approximation to the stress situation in a centrally cracked sheet specimen (with vertical and horizontal axes of symmetry of the specimen as y and x axes). The specimen, with width w = L is regarded to be one unit of the crack system (i. e., the plate with the system of cracks is regarded as being made up of a large number of centrally cracked specimens placed edge to edge). Thus the specimen edges are at $x = \pm L/2$ and the crack extends from $x = -a$ to $x = +a$.

Boundary conditions require the stresses σ_y and τ_{xy} to be zero along the borders of the crack and the stresses σ_x and τ_{xy} to be zero along the side boundries. All of these conditions are fulfilled except the condition that $\sigma_x = 0$ along the side boundary. Irwin has remedied the situation by rewriting σ_x as

$$\sigma_x = \text{Re } Z - y \text{ Im } Z' - \sigma_{ox} \quad [1]$$

where σ_{ox} is a constant stress adjusted so that

$$\int_0^\infty \sigma_x \, dy = o \qquad \text{at } x = \pm \frac{L}{2} .$$

The introduction of the constant σ_{ox} does not make σ_x zero everywhere along the side boundries, but it does reduce σ_x to a small value. We have assumed that this deviation from an exact solution is smaller than the relatively small errors introduced in practical application by the departure from linear elasticity theory at finite strains.

Irwin modified the equation giving displacement in the y direction to make it applicable to a generalized plane stress situation. The Irwin-Westergaard equation is

$$Ev = 2 \text{ Im } \overline{Z} - (1 + \nu) \, y \text{ Re } Z. \qquad \text{(B3)}$$

We will now take the Irwin-Westergaard equation and derive an expression for compliance at the specimen edges. The conditions at the edge of the specimen are $x = \pm L/2$ so that $z = \pm L/2 + iy$ where y will be 1/2 of the specimen gage length.

---

[1] Westergaard stated that an arbitrary constant stress could be applied in the x direction without disturbing the validity of the solution

The integration

$$\bar{Z} = \int Z \, dz$$

gives

$$\bar{Z} = -\frac{L\sigma}{\pi} \sin^{-1} \left(\frac{\cos \frac{\pi z}{L}}{\cos \frac{\pi a}{L}} \right) + C$$

where C is a complex constant of integration to be evaluated later using the known conditions at z = o.

Making use of the identities:

$$\cos \left[\frac{\pi}{L} \left(\frac{L}{2} + iy \right) \right] = -i \sinh \frac{\pi y}{L} ,$$

$$\sin \left[\frac{\pi}{L} \left(\frac{L}{2} + iy \right) \right] = \cosh \frac{\pi y}{L} ,$$

and

$$-\sin^{-1}(-im) = i \sinh^{-1}(m),$$

we find that

$$\bar{Z} = \frac{iL\sigma}{\pi} \sinh^{-1} \left[\frac{\sinh \frac{\pi y}{L}}{\cos \frac{\pi a}{L}} \right] + \text{Re } C + i \text{ Im } C$$

so that

$$\text{Im } \bar{Z} = \frac{L\sigma}{\pi} \sinh^{-1} \left[\frac{\sinh \frac{\pi y}{L}}{\cos \frac{\pi a}{L}} \right] + \text{Im } C.$$

We also see that at $x = \pm L/2$

$$Z = \frac{\sigma}{\sqrt{1 - \left(\frac{\sin \left(\frac{\pi a}{L} \right)}{\cosh \left(\frac{\pi y}{L} \right)} \right)^2}}$$

is real so that

$$\text{Re } Z = Z \qquad \text{at } x = \pm L/2.$$

We find the expression for displacement v by substitution into equation B3. Following Boyle (6) we express the compliance in the dimensionless form $Ev/\sigma w$ by multiplying the expression by the modulus of elasticity and dividing by the specimen width w.

Observing that L = w, we obtain

$$\frac{Ev}{\sigma w} = \frac{2}{\pi} \sinh^{-1}\left(\frac{\sinh \frac{\pi y}{w}}{\cos \frac{\pi a}{w}}\right) + \frac{2 \text{ Im } C}{\sigma w} - \frac{y}{w} \frac{(1+\nu)}{\sqrt{1 - \frac{\sin^2 \frac{\pi a}{w}}{\cosh^2 \frac{\pi y}{w}}}}.$$

Im C is evaluated by noting that at a = o the specimen corresponds to an unnotched specimen and $Ev/\sigma w$ is equal to y. w.

We obtain finally

$$\frac{Ev}{\sigma w} = \frac{2}{\pi} \sinh^{-1}\left(\frac{\sinh \frac{\pi y}{w}}{\cos \frac{\pi a}{w}}\right) - \frac{y}{w} \frac{(1+\nu)}{\sqrt{1 - \frac{\sin^2 \frac{\pi a}{w}}{\cosh^2 \frac{\pi y}{w}}}} + \frac{\nu y}{w}.$$